Meccanica (2009) 44: 741–765
DOI 10.1007/s11012-009-9210-6

Hall effects on MHD flow in a rotating system with heat transfer characteristics

S.K. Ghosh · O. Anwar Bég · M. Narahari

Received: 9 February 2008 / Accepted: 21 March 2009 / Published online: 1 April 2009

Abstract Closed-form solutions are derived for the steady magnetohydrodynamic (MHD) viscous flow in a parallel plate channel system with perfectly conducting walls in a rotating frame of reference, in the presence of Hall currents, heat transfer and a transverse uniform magnetic field. A mathematical analysis is described to evaluate the velocity, induced magnetic field and mass flow rate distributions, for a wide range of the governing parameters. Asymptotic behavior of the solution is analyzed for large M^2 (Hartmann number squared) and K^2 (rotation parameter). The heat transfer aspect is considered also with Joule and viscous heating effects present. Boundary layers arise close to the channel walls for large K^2, i.e. strong rotation of the channel. For slowly rotating systems (small K^2), Hall current parameter (m) reduces primary mass flow rate ($Q_x/R\rho v$). Heat transfer rate at the upper plate $(d\theta/d\eta)_{\eta=1}$ decreases, while at the lower plate $(d\theta/d\eta)_{\eta=-1}$ increases, with increase in either K^2 or m. For constant values of the rotation parameter, K^2, heat transfer rate at both plates exhibits an oscillatory pattern with an increase in Hall current parameter, m. The response of the primary and secondary velocity components and also the primary and secondary induced magnetic field components to the control parameters is also studied graphically. Applications of the study arise in rotating MHD induction machine energy generators, planetary and solar plasma fluid dynamics systems, magnetic field control of materials processing systems, hybrid magnetic propulsion systems for space travel etc.

Keywords MHD flow · Hall effects · Viscous effects · Asymptotic behavior · Heat transfer · MHD energy systems · Hartmann-Ekman boundary layers · Backflow · Secondary flow · Astrophysical plasma flows · Magneto-materials processing · Propulsion

Dedicated to the late Dr. Hannes O. G. Alfvén (May 30, 1908–April 2, 1995), Nobel Prize Winner in Physics (1970), for his monumental contributions to plasma physics and magnetohydrodynamics.

S.K. Ghosh (✉)
Magnetohydrodynamics Research Program, Applied Mathematics Section, Department of Mathematics, Narajole Raj College, P.O. Narajole, Midnapore (West), 721 211 West Bengal, India
e-mail: g_swapan2002@yahoo.com

O. Anwar Bég
Magneto-Fluid Dynamics, Biomechanics and Energy Systems Research, Mechanical Engineering Department, Sheaf Building, Sheffield Hallam University, Sheffield, S1 1WB, England, UK
e-mail: docoanwarbeg@hotmail.co.uk
e-mail: O.Beg@shu.ac.uk

M. Narahari
Heat Transfer Research, Department of Electrical and Electronics Engineering, Univertsiti Teknologi Petronas, 31750 Tronoh, Perak, Malaysia
e-mail: marneni@petronas.com.my

List of symbols

$\boldsymbol{q}$	velocity vector
$\boldsymbol{H}$	magnetic filed vector
$\boldsymbol{E}$	electric field vector
$\boldsymbol{J}$	current density vector
σ	electrical conductivity of Newtonian working fluid
ρ	fluid density
μ_e	magnetic permeability
ν	kinematic coefficient of viscosity
Ω	angular velocity
ω_e	cyclotron frequency
τ_e	electron collision time
M	Hartmann number
P_m	magnetic Prandtl number
R	dimensionless pressure gradient
K^2	rotation parameter which is the reciprocal of Ekman number
m	Hall current parameter
c_p	specific heat at constant pressure
K_1	thermal conductivity
P_r	Prandtl number
E_r	Eckert number

1 Introduction

Magnetohydrodynamic (MHD) flows have received wide attention from many researchers due to the significance of such flows in, for example, improved magnetohydrodynamic energy generators [1], planetary fluid dynamics [2], electromagnetic materials processing [3], control of crystal growth systems [4], lubrication control of high-speed spinning machine components with magnetic fields [5], magneto-astronautical flows [6] etc. MHD flow in a *rotating environment* may involve many complex fluid, thermophysical and electromagnetic effects including Coriolis forces, Lorentz retarding force, magnetic induction, boundary layer phenomena, flow reversal, strong thermal convection currents, viscous dissipation and Hall currents. Following the initiation of the subject of MHD in the seminal works of Alfven [7] in the 1940s, numerous engineering problems have been addressed in the past half century. Todd [8] studied the influence of high Hartmann number in annular hydromagnetic channel flow between two nonconducting cylinders of circular cross-section, identifying a divided core, wake generation at the boundaries of the various regions and for the case where the cylinders are eccentric, the presence of a net flow of current around the annulus. Vidyanidhi and Rao [9] analyzed the magnetohydrodynamic viscous incompressible flow in a straight pipe of circular cross-section under a constant pressure gradient with small angular velocity about the axis of rotation, presenting successive approximation solutions in ascending powers of the Hartmann number and computing stream lines in the central plane and the projection of the stream lines on the cross-section of the pipe. Nanda and Mohanty [10] obtained exact solutions for the MHD flow in a rotating channel, under constant transverse magnetic field, showing that for large values of the Hartmann number and the reciprocal of the Ekman number, thin boundary layers arise at the channel walls. Acheson and Hide [11] discussed rapidly rotating magnetohydrodynamic flows with a corotating magnetic field in the context of geophysical liquid core regimes. Mazumder [12] obtained closed-form solutions for the influence of wall conductance effects on hydromagnetic flow and heat transfer between rotating parallel plates showing that the velocity, current density and the temperature depend only on the sum of the wall conductances, whereas magnetic field depends on the individual values of these conductances. Prasad and Rao [13] investigated the hydromagnetic flow in a rotating channel with wall transpiration, under a constant pressure gradient, identifying that the flow is dependent on the Taylor number, pressure gradient, suction Reynolds number and the Hartmann number. It was shown also that when the Taylor number approaches infinity (for finite pressure gradients) thin boundary layers are formed close to the porous walls and increasing Hartmann number thins the boundary layers. Bhat [14] examined the MHD heat transfer in a rotating straight channel, showing that heat transfer rate decreases with an increase in the Hartmann number for weak rotation, but this effect is reversed for strong rotation. Singh and Tripathi [15] utilized the hodograph transformation to study the plane rotating viscous incompressible flows with orthogonal magnetic and velocity fields, considering both radial and vortex flow cases. Further studies of rotating viscous hydromagnetics have been communicated by Kumar et al. [16] who analyzed the rotating disk with surface transpiration, Nagy and Demendy [17] who studied the effect of wall conductance on spinning Hartmann

flow and heat transfer, Ghosh [18] who reported on the effects of periodic pressure gradient and Ghosh and Pop [19] who studied the effect of an inclined magnetic field. More recently Asghar et al. [20] studied analytically hydromagnetic rotating viscoelastic flow with applications in materials processing. Roy et al. [21] studied numerically the transient hydromagnetic boundary layer thermal convection flow from an infinite permeable rotating cone in a rotating fluid with applied constant magnetic field. They simulated unsteadiness via the time-dependent angular velocity of the body, as well as that of the fluid and found that magnetic field, surface velocity, and suction and injection strongly influence the local skin friction coefficients in both tangential and azimuthal directions. This study further identified that when the angular velocity of the fluid is greater than that of the body, the velocity profiles tend to their asymptotic values at the edge of the boundary layer in an oscillatory manner, although both suction (transpiration) and magnetic field significantly suppress these oscillations. Hayat et al. [22] obtained exact analytic solutions for second order hydromagnetic flow due to non-coaxial rotations of a porous disk and a fluid at infinity and also for the magnetohydrodynamic flow of a second order fluid in a rotating channel with transpiration effects along the axial direction, using perturbation methods. They showed that an asymptotic solution exists for the velocity both in the case of suction and blowing. Xu and Liao [23] derived series solutions for unsteady hydromagnetic flow generated by an impulsively rotating infinite disk using the homotopy analysis method. Asghar et al. [24] have considered the effects of slip (of interest in micro-device technology) on transient magnetohydrodynamic flow due to non-coaxial rotations of disk and a fluid at infinity using the Laplace transform method for a wide range of magnetic field and slip parameter values.

The above studies neglected the important effect of *Hall currents*. Lighthill [25] was the first to highlight the need to incorporate this effect in magnetohydrodynamic flows owing to the strong influence it can exert on flow distributions, for example in magnetic fusion systems, electrically-conducting aerodynamics, energy generators etc. Hall-magnetohydrodynamics (HMHD) takes into account this electric field description of magnetohydrodynamics. The key difference from classical MHD studies is that in the absence of field line breaking, the magnetic field is tied to the electrons and not to the bulk fluid. Sato [26] presented the first significant study of Hall current effects on magnetohydrodynamic boundary layers, showing that the flow becomes *secondary* in nature. Subsequently significant interest has been stimulated in the context of developing efficient Hall thrusters in magnetic propulsion [27], plasma actuator control of hypersonic flows [28] and materials processing exploiting Hall currents [29]. Nishihara et al. [30] discussed magnetohydrodynamic (MHD) boundary layer control experiments using repetitively pulsed, short-pulse duration, high-voltage discharges in supersonic flows of nitrogen and air in the presence of a magnetic field of 1.5 Tesla with Hall current effects. Boundary-layer separation has also been shown to be magnified near the anode in pulsed MHD generators due to the strong Lorentz force attributed to large Hall current [27]. Excellent studies of Hall current effects in *rotating* MHD flows have been presented by Seth and Ghosh [31] who considered asymptotic behaviour of rotating channel hydromagnetics with Hall current, Linga Raju and Rao [32] who studied Hall effects on rotating ionized magneto-heat transfer, Ram et al. [33] who considered both Hall and ionslip current effects with periodic thermal boundary conditions at the wall, Takhar et al. [34, 35] who discussed impulsive and free stream effects, Ghosh [36] who considered arbitrary magnetic field effects in rotating MHD Couette flow and Ghosh and Pop [37, 38] who studied periodic pressure gradient and Hall effects. Hayat et al. [39] extended the analysis by Ghosh [36] to examine non-Newtonian effects. Naroua [40] studied numerically both Hall and ionslip effects on heat generating natural convection rotating flow. Naroua et al. [41] extended the model in [40] to examine in more detail heat generation and Hall current effects on flow and temperature distributions. Very recently Bég et al. [42] analyzed using network analysis the combined effects of Ohmic dissipation, Hall and ionslip currents on transient hydromagnetic flow in a porous medium channel. The purpose of the present investigation is to study *Hall current effects on MHD flow in a rotating configuration with perfectly conducting walls and its heat transfer characteristics*; such a study has immediate applications in MHD energy generators and has to the knowledge of the authors, not received attention in the engineering sciences literature thus far.

2 Mathematical model

Consider the steady MHD fully developed flow of an electrically-conducting, viscous, incompressible fluid confined between two horizontal perfectly conducting parallel plates orientated at $y = \pm L$, rotating with an uniform angular velocity Ω about an axis perpendicular to the plane of flow in the presence of a constant pressure gradient along the x-direction and a uniform magnetic field H_0 applied parallel to the y-axis, about which both the fluid and channel rotate in unison with the same constant angular velocity Ω, as shown in Fig. 1. Since the plates are infinite along the x- and z-directions all physical quantities except pressure will be the functions of y only. The following assumptions are compatible with the fundamental equations of magnetohydrodynamics, following Sutton and Sherman [43]:

$$\begin{aligned} &\boldsymbol{q} = (u, 0, w); \qquad \boldsymbol{H} = (H_x, H_0, H_z) \\ &\boldsymbol{E} = (E_x, E_y, E_z); \qquad \boldsymbol{J} = (J_x, 0, J_z) \end{aligned} \tag{1}$$

where $\boldsymbol{q}$, $\boldsymbol{H}$, $\boldsymbol{E}$ and $\boldsymbol{J}$ are the velocity vector, magnetic field vector, electric field vector and current density vector, respectively. The effects of Hall current become significant when the applied magnetic field is strong enough, as encountered in Hall MHD generators, plasma thrusters. The magnetic induction equation also has to be modified to include Hall current effects. With the above assumptions, the MHD momentum equation can be written in a component form as follows:

$$2\Omega w = -\frac{1}{\rho}\frac{\partial p}{\partial x} + v\frac{\partial^2 u}{\partial y^2} + \frac{\mu_e H_O}{\rho}\frac{\partial H_x}{\partial y}, \tag{2}$$

$$0 = -\frac{1}{\rho}\frac{\partial p}{\partial y} - \frac{\mu_e}{\rho}\left(H_X\frac{\partial H_X}{\partial y} + H_Z\frac{\partial H_Z}{\partial y}\right), \tag{3}$$

$$-2\Omega u = v\frac{\partial^2 w}{\partial y^2} + \frac{\mu_e H_O}{\rho}\frac{\partial H_Z}{\partial y}. \tag{4}$$

The magnetic induction equation can be written in component form including Hall current effects as follows:

$$-\frac{\partial^2 H_X}{\partial y^2} + \omega_e\tau_e\frac{\partial^2 H_Z}{\partial y^2} = \sigma\mu_e H_O\frac{\partial u}{\partial y} \tag{5}$$

$$-\frac{\partial^2 H_Z}{\partial y^2} - \omega_e\tau_e\frac{\partial^2 H_X}{\partial y^2} = \sigma\mu_e H_O\frac{\partial w}{\partial y} \tag{6}$$

where $\sigma, \rho, \mu_e, \nu, \Omega, \omega_e$ and τ_e are, respectively, the electrical conductivity, fluid density, magnetic permeability, kinematic coefficient of viscosity, angular velocity, cyclotron frequency and the electron collision time. Introducing dimensionless variables:

$$\begin{aligned} &\eta = y/L, \quad u_1 = uL/v, \\ &w_1 = wL/v, \quad h_x = H_X/\sigma\mu_e v H_O, \\ &h_z = H_z/\sigma\mu_e v H_O, \quad p^* = L^2 p/\rho v^2, \quad x = \xi^* L \end{aligned} \tag{7}$$

the partial differential conservation equations (2) to (6) reduce to the following set of equations in terms of the transformed independent space variable, η:

$$\frac{d^2 u_1}{d\eta^2} + M^2\frac{dh_X}{d\eta} - 2K^2 w_1 = -R, \tag{8}$$

$$\frac{\partial p^*}{\partial \eta} + P_m M^2\left(h_X\frac{dh_X}{d\eta} + h_z\frac{dh_z}{d\eta}\right) = o, \tag{9}$$

$$\frac{d^2 w_1}{d\eta^2} + M^2\frac{dh_z}{d\eta} + 2K^2 u_1 = o, \tag{10}$$

$$-\frac{d^2 h_x}{d\eta^2} + m\frac{d^2 h_z}{d\eta^2} = \frac{du_1}{d\eta}, \tag{11}$$

$$-\frac{d^2 h_z}{d\eta^2} - m\frac{d^2 h_x}{d\eta^2} = \frac{dw_1}{d\eta} \tag{12}$$

in which $M = \mu_e H_o L(\sigma/\rho\nu)^{1/2}$ is the Hartmann (magnetofluid dynamic) effect number, $P_m = \sigma\mu_e\nu$ is the magnetic Prandtl number, $R = -\partial p^*/\partial\xi^*$ is the dimensionless pressure gradient along the x-direction (which is a constant), $K^2 = \Omega L^2/\nu$ is the rotation parameter (reciprocal of the Ekman number) and $m = \omega_e\tau_e$ is the Hall current parameter. Since the plates of the channel are *perfectly* conducting the boundary conditions become:

$$u_1 = w_1 = 0 \qquad \text{at } \eta = \pm 1, \tag{13}$$

$$\frac{dh_x}{d\eta} = \frac{dh_z}{d\eta} = 0 \quad \text{at } \eta = \pm 1. \tag{14}$$

Since the fields will be symmetric about the mid plane $\eta = 0$, we consider the half space region, $\eta = 0$ to $\eta = 1$. The boundary conditions at $\eta = -1$ can be replaced by the symmetry conditions at $\eta = 0$, viz.

$$\frac{du_1}{d\eta} = \frac{dw_1}{d\eta} = 0 \quad \text{at } \eta = 0, \tag{15a}$$

$$h_x = h_z = 0 \qquad \text{at } \eta = 0. \tag{15b}$$

3 Analytical solutions

Combining (8) and (10) together with (11) and (12) respectively, we obtain:

$$\frac{d^2F}{d\eta^2} + M^2\frac{dH}{d\eta} + 2iK^2F = -R \tag{16}$$

$$\frac{d^2H}{d\eta^2} + \frac{1}{1+im}\frac{dF}{d\eta} = 0 \tag{17}$$

where $F = u_1 + iw_1$ and $H = h_x + ih_z$. The corresponding boundary conditions are

$$\frac{dF}{d\eta} = 0 \quad \text{at } \eta = 0, \qquad F = 0 \quad \text{at } \eta = \pm 1 \tag{18}$$

$$H = 0 \quad \text{at } \eta = 0, \qquad \frac{dH}{d\eta} = 0 \quad \text{at } \eta = 1. \tag{19}$$

Equations (16) and (17) together with the boundary conditions (18) and (19) can be solved and the velocity and induced magnetic field functions can be expressed as:

$$F(\eta) = R\frac{(\alpha+i\beta)^2}{(\alpha^2+\beta^2)^2}\left[1 - \frac{\cosh(\alpha-i\beta)\eta}{\cosh(\alpha-i\beta)}\right], \tag{20}$$

$$H(\eta) = R\left(\frac{1-im}{1+m^2}\right)\frac{(\alpha+i\beta)^2}{(\alpha^2+\beta^2)^2} \times \left[\frac{\sinh(\alpha-i\beta)\eta}{(\alpha-i\beta)\cosh(\alpha-i\beta)} - \eta\right], \tag{21}$$

where

$$\alpha = \frac{1}{\sqrt{2}}\left[\left\{\frac{M^4}{1+m^2} + \frac{4m}{1+m^2}M^2K^2 + 4K^4\right\}^{1/2} + \frac{M^2}{1+m^2}\right]^{1/2}, \tag{22a}$$

$$\beta = \frac{1}{\sqrt{2}}\left[\left\{\frac{M^4}{1+m^2} + \frac{4m}{1+m^2}M^2K^2 + 4K^4\right\}^{1/2} - \frac{M^2}{1+m^2}\right]^{1/2}. \tag{22b}$$

3.1 Shear stresses

Next we evaluate the shear stresses at the plates, at $\eta = \pm 1$. The non-dimensional shear stresses τ_x/R and τ_Z/R at the plates $\eta = \pm 1$ due to *primary* and *secondary* flows respectively are:

$$\tau_X/R = \frac{1}{(\alpha^2+\beta^2)}\left[\mp\left(\frac{\alpha\sinh 2\alpha + \beta\sinh 2\beta}{\cosh 2\alpha + \cos 2\beta}\right)\right], \tag{23}$$

$$\tau_Z/R = \frac{1}{(\alpha^2+\beta^2)}\left[\mp\left(\frac{\beta\sinh 2\alpha - \alpha\sinh 2\beta}{\cosh 2\alpha + \cos 2\beta}\right)\right], \tag{24}$$

where the upper and lower signs in (23) and (24) represent the values at the upper plate ($\eta = 1$) and that at the lower plate ($\eta = -1$) respectively. We note from (23) and (24) that the shear stress components τ_X/R and τ_Z/R due to primary and secondary flows respectively vanish neither at the upper plate nor at the lower plate. Thus we arrive at an interesting conclusion that for perfectly conducting plates there is *no backflow* in either the primary and secondary flow fields.

3.2 Mass flow rate

If $Q_X/R\rho\nu$ and $Q_Z/R\rho\nu$ denote the mass flow rates in the x and z-directions respectively, then we have:

$$\frac{Q_X + iQ_Z}{R\rho\nu} = \frac{(\alpha-\iota\beta)^3}{(\alpha^2+\beta^2)^3}\left[(\alpha-\iota\beta) - \tanh(\alpha-\iota\beta)\right]. \tag{25}$$

In the absence of rotation, the problem reduces to the *flow through a straight channel in the presence of a constant pressure gradient with Hall effects under a transverse magnetic field*. The solutions for the velocity and induced magnetic field may be obtained by setting $K^2 = 0$ in (20) and (21) which are given by:

$$F(\eta) = R\frac{(\alpha+i\beta)^2}{(\alpha^2+\beta^2)^2}\left[1 - \frac{\cosh(\alpha-i\beta)\eta}{\cosh(\alpha-i\beta)}\right], \tag{26}$$

$$H(\eta) = R\frac{(1-im)}{(1+m^2)}\frac{(\alpha+i\beta)^2}{(\alpha^2+\beta^2)^2} \times \left[\frac{\sinh(\alpha-i\beta)\eta}{(\alpha-i\beta)\cosh(\alpha-i\beta)} - \eta\right], \tag{27}$$

where

$$\alpha = M\frac{[(1+m^2)^{1/2}+1]^{1/2}}{[2(1+m^2)]^{1/2}}, \qquad \beta = M\frac{[(1+m^2)^{1/2}-1]^{1/2}}{[2(1+m^2)]^{1/2}}. \tag{28}$$

4 Asymptotic solutions

We shall now discuss asymptotic behavior of the solutions given by (20) and (21) to garner a physical insight into the flow dynamics.

Case I: $M^2 \ll 1$ and $K^2 \ll 1$

Since M^2 and K^2 are very small, neglecting squares and higher powers of M^2 and K^2 in (20) and (21) we obtain the velocity and induced magnetic field components as:

$$u_1/R = \frac{1}{2}(1-\eta^2) + \frac{M^2}{1+m^2} \times \left(-\frac{5}{24} + \frac{1}{4}\eta^2 - \frac{1}{24}\eta^4\right) + \cdots, \tag{29}$$

$$w_1/R = \left(2K^2 - \frac{mM^2}{1+m^2}\right) \times \left(-\frac{5}{24} + \frac{1}{4}\eta^2 - \frac{1}{24}\eta^4\right) + \cdots, \tag{30}$$

$$h_X/R = \frac{1}{2}\left(-\eta + \frac{1}{3}\eta^3\right) + \frac{M^2}{12(1+m^2)} \times \left(\frac{5}{2}\eta + \frac{1}{10}\eta^5 - \eta^3\right) + \cdots, \tag{31}$$

$$h_Z/R = \frac{1}{12}\left(2K^2 - \frac{mM^2}{1+m^2}\right) \times \left(\frac{5}{2}\eta + \frac{1}{10}\eta^5 - \eta^3\right) + \cdots \tag{32}$$

It is evident from the expressions (29) to (32) that in a *slowly* rotating system when the electrical conductivity of the fluid is low and the applied magnetic field is weak, the secondary flow given by w_1/R and the induced magnetic field h_z/R are strongly affected by rotation (K^2), Hall current (m) and applied magnetic field (M^2), while the primary flow as given by u_1/R and the induced magnetic field h_x/R are *independent* of rotation (K^2).

In the absence of Hall current ($m = 0$) the problem reduces to the *steady hydromagnetic flow in a rotating channel* and the corresponding solutions degenerate to:

$$u_1/R = \frac{1}{2}(1-\eta^2) + M^2\left(-\frac{5}{24} + \frac{1}{4}\eta^2 - \frac{1}{24}\eta^4\right) + \cdots, \tag{33}$$

$$w_1/R = K^2\left(-\frac{5}{12} + \frac{1}{2}\eta^2 - \frac{1}{12}\eta^4\right) + \cdots, \tag{34}$$

$$h_x/R = \frac{1}{2}\left(-\eta + \frac{1}{3}\eta^3\right) + \frac{M^2}{12}\left(\frac{5}{2}\eta + \frac{1}{10}\eta^5 - \eta^3\right) + \cdots, \tag{35}$$

$$h_z/R = \frac{1}{6}K^2\left(\frac{5}{2}\eta - \eta^3 + \frac{1}{10}\eta^5\right) + \cdots. \tag{36}$$

These are exactly in agreement with those obtained by Nanda and Mohanty [10]. Inspection of expressions (29) to (32) indicates that in the absence of Hall current, rotation and magnetic field, the problem reduces to *classical viscous hydrodynamic flow through a straight channel under a constant pressure gradient* and our solutions reduce to the classical result:

$$u_1/R = \frac{1}{2}\left(1-\eta^2\right), \qquad w_1/R = 0. \tag{37}$$

Case II: $K^2 \gg 1$ and $M^2 \sim O(1)$

When K^2 is large and M^2 is of small order-of-magnitude the flow attains a boundary-layer nature. For the boundary layer at the wall $\eta = 1$, we write $(1-\eta) = \xi$ and we obtain from the solutions (20) and (21) the following:

$$u_1/R = \frac{1}{2K^2}e^{-\alpha_1\xi}\sin\beta_1\xi, \tag{38}$$

$$w_1/R = \frac{1}{2K^2}(1 - e^{-\alpha_1\xi}\cos\beta_1\xi), \tag{39}$$

$$h_x/R = -\frac{1}{2\sqrt{2}K^3}\left[\left\{\frac{1}{(1+m^2)}e^{-\alpha_1\xi}\sin(\beta_1\xi + \pi/4) + \frac{m}{(1+m^2)}e^{-\alpha_1\xi}\sin(\beta_1\xi - \pi/4)\right\} + \frac{\sqrt{2}Km}{(1+m^2)}(\xi - 1)\right], \tag{40}$$

$$h_z/R = \frac{1}{2K^3}\left[\frac{K}{(1+m^2)}(1-\xi) + \frac{1}{\sqrt{2}}\left\{\begin{array}{l}\frac{m}{(1+m^2)}e^{-\alpha_1\xi}\sin(\beta_1\xi + \pi/4) \\ -\frac{1}{(1+m^2)}e^{-\alpha_1\xi}\sin(\beta_1\xi - \pi/4)\end{array}\right\}\right], \tag{41}$$

in which:

$$\alpha_1 = K\left\{1+\left(\frac{1-m}{1+m^2}\right)\frac{M^2}{4K^2}\right\},$$
$$\beta_1 = K\left\{1-\left(\frac{1+m}{1+m^2}\right)\frac{M^2}{4K^2}\right\}. \tag{42}$$

Expressions (38) to (41) demonstrate the existence of a *thin boundary layer* of thickness $O\{K(1+\frac{1-m}{1+m^2}\frac{M^2}{4K^2})\}^{-1}$ near the plate of the channel. The thickness of the boundary layer decreases with increase in either K^2 or M^2. This boundary layer may be identified as the *modified hydromagnetic Ekman layer*. The exponential terms in the expressions (38) to (41) damp out quickly as ξ increases. When $\xi \geq 1/\alpha_1$ i.e. outside the boundary layer region, we have:

$$u_1/R \approx 0, \qquad w_1/R \approx \frac{1}{2K^2}, \tag{43}$$

$$h_x/R \approx \frac{m(1-\xi)}{2K^2(1+m^2)}, \qquad h_z/R \approx \frac{(1-\xi)}{2K^2(1+m^2)}. \tag{44}$$

It is evident from expressions (43) and (44) that in a certain core, given by $\xi \geq 1/\alpha_1$, about the axis of the channel, the velocity in the direction of the pressure gradient vanishes away but it persists in the y-direction. Thus, in the central core, the fluid will be moving in the direction of the pressure gradient only. It is noticed from (44) that the primary and secondary induced magnetic fields h_x/R and h_z/R, respectively, decrease with increase in ξ and at the central line of the channel vanish. Thus we conclude that there is a possibility of *current-free zone* near the central line of the channel. Also expression (44) shows that the induced magnetic field components are independent of Hartmann number M but, are sensitive to the effects of rotation and Hall current.

Case III: $M^2 \gg 1$ and $K^2 \sim 0(1)$

In this case, the flow also has a *boundary-layer type* character and we obtain from (20) and (21):

$$\frac{u_1}{R} = \frac{1}{M^2}\left[1-e^{-\frac{M}{\sqrt{1+m^2}}\xi}\left\{1-\frac{m^2}{8(1+m^2)}M^2\xi\right\}\right], \tag{45}$$

$$\frac{w_1}{R} = \frac{\sqrt{1+m^2}}{2M^3}e^{-\frac{M}{\sqrt{1+m^2}}\xi}\left(2K^2-\frac{mM^2}{1+m^2}\right)\xi, \tag{46}$$

$$\frac{h_x}{R} = \frac{1}{M^3(1+m^2)}e^{-\frac{M}{\sqrt{1+m^2}}\xi}\left(1-\frac{m^2}{8(1+m^2)}M^2\xi\right) + \frac{m}{2M^4\sqrt{1+m^2}}e^{-\frac{M}{\sqrt{1+m^2}}\xi}\xi \times\left(\frac{mM^2}{1+m^2}-2K^2\right)-\frac{(1-\xi)}{M^2(1+m^2)} \tag{47}$$

$$\frac{h_z}{R} = \frac{1}{2M^4\sqrt{(1+m^2)}}e^{-\frac{M}{\sqrt{1+m^2}}\xi}\left(\frac{mM^2}{1+m^2}-2K^2\right)\xi - \frac{m}{M^3(1+m^2)}e^{-\frac{M}{\sqrt{1+m^2}}\xi}\left(1-\frac{m^2M^2}{8(1+m^2)}\xi\right) + \frac{m}{M^2(1+m^2)}(1-\xi) \tag{48}$$

It is evident from expressions (45) to (48) that there arises a *thin boundary layer* of thickness, $0(\frac{M}{\sqrt{1+m^2}})^{-1}$ near the plate of the channel. This layer may be identified as the modified Hartmann layer. The thickness of this layer increases with increase in Hall parameter, m, while it decreases with increase in Hartmann number M. In a certain core, given by $\xi \geq (\frac{M}{\sqrt{1+m^2}})^{-1}$:

$$u_1/R \approx 1/M^2, \qquad w_1/R \approx 0, \tag{49}$$

$$h_x/R \approx -\frac{(1-\xi)}{M^2(1+m^2)}, \qquad h_z/R \approx \frac{m(1-\xi)}{M^2(1+m^2)}. \tag{50}$$

Expression (49) reveals that, outside the boundary layer region, the secondary velocity disappears while primary velocity persists and is independent of Hall current, rotation and ξ. Thus fluid will be moving in the direction of pressure gradient only and the primary velocity in the central core is uniform with respect to the channel width. Expression (50) shows that there is no effect of rotation on the induced magnetic fields h_X/R and h_z/R in the main body of the flow whereas they are affected by Hall current and magnetic field. Also these quantities vary linearly with η and disappear at the central line of the channel indicating a current free zone near the central axis.

5 Heat transfer characteristics

We shall now discuss heat transfer characteristics of the flow regime for the specific case where the upper

and lower plates of the channel are maintained at uniform temperatures T_1 and T_0 respectively. The energy equation for steady hydromagnetic fully-developed flow, including viscous and Joule (Ohmic) dissipations can be presented as the following *ordinary* differential equation:

$$0 = \alpha^* \frac{d^2T}{dy^2} + \frac{v}{c_p}\left\{\left(\frac{du}{dy}\right)^2 + \left(\frac{dw}{dy}\right)^2\right\} + \frac{1}{c_p\sigma}\left\{\left(\frac{dH_X}{dy}\right)^2 + \left(\frac{dH_Z}{dy}\right)^2\right\} \tag{51}$$

in which T is the temperature of the fluid taken as a function of y only, $\alpha^* = K_1/\rho c_P$ (K_1 denoting thermal conductivity of the conducting fluid) and the other symbols have their usual meanings. The boundary conditions for the temperature field are:

$$\begin{aligned} &T = T_0 \quad \text{at } y = -L \quad \text{and} \\ &T = T_1 \quad \text{at } y = L (T_0 < T < T_1). \end{aligned} \tag{52}$$

Using the dimensionless variables (7) and introducing supplementary dimensionless quantities:

$$\theta(\eta) = (T - T_0)/(T_1 - T_0), \qquad E_r = v^2/L^2 C_P (T_1 - T_0), \qquad P_r = v/\alpha^*.$$

Implementation in (51) leads to the normalized version of the energy conservation equation, viz:

$$\frac{d^2\theta}{d\eta^2} + P_r E_r\left[\left\{\left(\frac{du_1}{d\eta}\right)^2 + \left(\frac{dw_1}{d\eta}\right)^2\right\} + M^2\left\{\left(\frac{dh_x}{d\eta}\right)^2 + \left(\frac{dh_z}{d\eta}\right)^2\right\}\right] = 0, \tag{53}$$

where P_r and E_r are Prandtl number and Eckert number respectively, the latter signifying the ratio of kinetic energy of the flow to the boundary layer enthalpy difference. The boundary conditions (52) transform to:

$$\theta(-1) = 0 \quad \text{and} \quad \theta(1) = 1. \tag{54}$$

Substituting the values of $u_1(\eta)$, $w_1(\eta)$, $h_x(\eta)$ and $h_z(\eta)$ from (20) and (21) in (53) and solving the resulting equation subject to the boundary conditions (54) we obtain:

$$\begin{aligned} \theta(\eta) = {} & \frac{1}{2}(1+\eta) \\ & - P_r E_r\left\{C_{16}\cosh 2\alpha\eta + C_{17}\cos 2\beta\eta \right. \\ & + C_{14}(\beta\sinh\alpha\eta\sin\beta\eta + \alpha\cosh\alpha\eta\cos\beta\eta) \\ & - C_{15}(\alpha\sinh\alpha\eta\sin\beta\eta - \beta\cosh\alpha\eta\cos\beta\eta) \\ & \left. + C_5\frac{\eta^2}{2}\right\} + P_r E_r\left\{C_{16}\cos 2\alpha + C_{17}\cos 2\beta \right. \\ & + C_{14}(\beta\sinh\alpha\sin\beta + \alpha\cosh\alpha\cosh\beta) \\ & - C_{15}(\alpha\sinh\alpha\sin\beta - \beta\cosh\alpha\cosh\beta) \\ & \left. + \frac{1}{2}C_5\right\}, \end{aligned} \tag{55}$$

where $C_5, \ldots C_i$ ($i = 14$, 15, 16 and 17) are known functions of M^2, K^2 and m, and are given in the Appendix. The expressions for *the rate of heat transfer* at both the plates are also derived. We omit these expressions, as they are quite lengthy.

6 Results and discussion

We have computed the variation of primary and secondary shear stresses at the upper plate (τ_x, τ_z), primary and secondary mass flow rates ($Q_x/R\rho v$, $Q_z/R\rho v$) and also the heat transfer rates at the upper and lower plates for a wide range of K^2 and m values, for a strong magnetic field ($M^2 = 10$). These are provided in Tables 1 to 6. Additionally the evolution of dimensionless velocities (u_1, w_1) and induced magnetic field components (h_x, h_z) across the channel width for different values of rotation parameter (K^2) and Hall current parameter (m) with constant Hartmann number ($M^2 = 10$) and constant pressure gradient ($R = 1$) are shown in the Figs. 2 to 6. Throughout the Prandtl number is held constant at $P_r = 0.25$ (corresponding to partially ionized water) and the Eckert number maintained at $E_r = 2.0$ (very strong viscous dissipation effects).

Inspection of *Table* 1 reveals that, for *low* rotation values (i.e. high viscous force compared with the Coriolis force), the primary and secondary shear stresses τ_x/R and τ_z/R at $\eta = 1$ increase in magnitude with increase in m for any value of K^2. The primary shear stress values are consistently negative indicating that back flow is generated in the primary flow; conversely the secondary shear stresses are always positive. This is in logical agreement with the secondary nature of

Table 1 Shear stresses τ_x/R and τ_z/R at the plate $\eta = 1$ for $M^2 = 10$

K^2	m					
	τ_x/R			τ_z/R		
	0.5	1.0	1.5	0.5	1.0	1.5
1	−0.34404	−0.39893	−0.47037	0.04085	0.10268	0.14914
3	−0.34406	−0.43229	−0.51550	0.04035	0.03861	0.09009
5	−0.30107	−0.35160	0.35815	0.09885	0.14025	0.20019

Table 2 Shear stresses τ_x/R and τ_z/R at the plate $\eta = 1$ for $M^2 = 10$

K^2	m					
	τ_x/R			τ_z/R		
	0.5	1.0	1.5	0.5	1.0	1.5
75	−0.06005	−0.05971	−0.05926	0.05685	0.05768	0.05801
81	−0.05762	−0.05731	−0.05691	0.05478	0.05551	0.05581
90	−0.05447	−0.05419	−0.05385	0.05205	0.05267	0.05292

Table 3 Mass flow rates $Q_x/R\rho\nu$ and $Q_2/R\rho\nu$ for $M^2 = 10$

K^2	m					
	$Q_x/R\rho\nu$			$Q_z/R\rho\nu$		
	0.5	1.0	1.5	0.5	1.0	1.5
1	0.06772	0.03109	−0.02494	−0.01214	−0.10102	−0.14082
3	0.06771	0.00938	−0.06818	−0.042114	−0.05138	−0.13477
5	0.00984	−0.02113	−0.08249	−0.07003	−0.03233	−0.07276

Table 4 Mass flow rates $Q_x/R\rho\nu$ and $Q_z/R\rho\nu$ for $M^2 = 10$

K^2	m					
	$Q_x/R\rho\nu$			$Q_z/R\rho\nu$		
	0.5	1.0	1.5	0.5	1.0	1.5
75	−0.00643	−0.00649	−0.00648	−0.00032	−0.00005	0.00012
81	−0.00597	−0.00601	−0.00600	−0.00026	−0.00003	0.00012
90	−0.00537	−0.00541	−0.00540	−0.00019	−0.00008	0.00011

the Hall current effect which will benefit the secondary flow in the regime. For $K^2 = 1$ the Coriolis and viscous forces are of the same order of magnitude and the *Hartmann-Ekman boundary layers* will be formed at the plate (analogous to the formation of *Ekman boundary layers* in *purely hydrodynamic rotating flow*). For both $K^2 = 1$ and 3, primary shear stress becomes increasingly negative as m increases; however for $K^2 = 5$ there is a dramatic change from backflow to normal flow from $m = 1.0$ to $m = 1.5$. This indicates that there exists a *critical Hall current* (m value) for which primary flow switches from deceleration to acceleration, an important feature in practical MHD energy generator operations. Secondary flow is accelerated for $K^2 = 1$ (it increases continuously from 0.04085 through 0.10266 to 0.14914, as m increases from 0.5 through 1 to 1.5). However for $K^2 = 3$, secondary flow has an oscillatory response; τ_z/R de-

Table 5 The rate of heat transfer $(d\theta/d\eta)\eta = \pm 1$ for $M^2 = 10$, $R = 1$, $P_r = 0.25$ and $E_r = 2.0$

m	K^2					
	$(d\theta/d\eta)\eta = 1$			$(d\theta/d\eta)\eta = -1$		
	0.5	1.0	1.5	0.5	1.0	1.5
1	0.47726	0.47158	0.46356	0.52274	0.52842	0.53644
3	0.46385	0.44586	0.39431	0.53614	0.55413	0.60569
5	0.43844	0.40436	0.37730	0.56156	0.59564	0.62269

Table 6 The rate of heat transfer $(d\theta/d\eta)\eta = \pm 1$ for $M^2 = 10$, $R = 1$, $P_r = 0.25$ and $E_r = 2.0$

m	K^2					
	$(d\theta/d\eta)\eta = 1$			$(d\theta/d\eta)\eta = -1$		
	0.5	1.0	1.5	0.5	1.0	1.5
75	0.41849	0.41779	0.41796	0.58151	0.58220	0.58204
81	0.41861	0.41797	0.41813	0.58139	0.58202	0.58187
90	0.41876	0.41820	0.41834	0.58124	0.58179	0.58166

creases from 0.04035 to 0.03861 and then rises again to the maximum value of 0.09009. For the highest value of K^2, the secondary shear stress increases continuously with m values. We note that the primary flow is generally an order of magnitude greater than the secondary flow. In Table 2, again primary and secondary shear stress values are tabulated, this time for much greater values of the rotation (inverse Ekman) parameter. Again we observe a strong flow reversal for all values of m in the primary flow; no such reversal is apparent in the secondary flow. Magnitudes of the primary shear stress are however much smaller than for Table 1, indicating that greater rotation stifles backflow considerably. For the secondary flow, there is a consistent increase in τ_z/R values with increasing Hall current parameter, m. However the change is very small as compared with the response at lower rotation values. We deduce therefore that intensive rotation is counter-productive compared with weak rotation, with regard to the secondary flow. Table 3 reveals that, for low rotation, primary mass flow rate $Q_x/R\rho v$ decreases with increase in either K^2 or m and the secondary mass flow rate $Q_z/R\rho v$ increases with m when $K^2 < 5$ whereas the secondary mass flow rate $Q_x/R\rho v$ increases in magnitude with increase in K^2 when $m = 0.5$. We note that for $m = 1.5$, back flow is actually increased in the primary flow with an increase in K^2, whereas for $K^2 = 1$ (equivalent order of magnitude of the viscous and Coriolis forces), the largest value of K^2 actually induces backflow not present for lower K^2 values. Backflow is experienced for all values of the Hall current parameter, m, in the secondary flow; it is amplified with a rise in K^2 for $m = 0.5$, but suppressed with an increase in K^2 for $m = 1.0$ and $m = 1.5$. Table 4 shows that, for high rotation ($K^2 = 75, 81, 90$), mass flow rates $Q_z/R\rho v$ and $Q_z/R\rho v$ demonstrate an oscillatory character with an increase in Hall current parameter, m; for fixed m, the primary and secondary mass flow rates $Q_x/R\rho v$ and $Q_z/R\rho v$ decrease in magnitude with increase in K^2. This implies that, in a slowly rotating system, Hall current retards the mass flow rate in the primary flow while, for rapidly rotating system, rotation retards the mass flow rate in the secondary flow. We further identify that backflow occurs in *every* case of high K^2 values, with the exception of the maximum Hall current in the secondary flow i.e. $m = 1.5$, where the secondary flow is decelerated but not reversed. Examination of Table 5 indicates that, for low rotation ($K^2 = 1, 3, 5$), the rate of heat transfer, at the upper plate i.e $(d\theta/d\eta)_{\eta=1}$ decreases with increase in either K^2 or m. Maximum heat transfer rate therefore corresponds to the weakest rotation and Hall current values ($K^2 = 1, m = 0.5$). Conversely rate of heat transfer, at the lower plate i.e. $(d\theta/d\eta)_{\eta=-1}$ increases continuously with m and K^2 values; maximum heat transfer rate at the lower plate therefore is associated with

$K^2 = 5$ and $m = 1.5$. Hall currents and stronger rotational velocity therefore oppose the *conduction* of heat from the upper plate into the fluid (for *positive Eckert number* heat is transported from the plate to the fluid; the negative Eckert number case is not considered here) and will cause a decrease in fluid regime temperature in the vicinity of the lower plate; the converse will occur at the lower plate where greater thermal energy will be transferred from the lower plate to the fluid. It is noticed from Table 6 that, for high rotation, the rate of heat transfer at the upper plate increases with increase in K^2 whereas, at the lower plate, it decreases with increase in K^2 for fixed m. This is the opposite trend to that in Table 5 for weak rotation. For fixed K^2, the rate of heat transfer at both the plates behaves in oscillatory manner with an increase in Hall current parameter, m. Thus we conclude that, for low rotation, rotation and Hall current reduce the rate of heat transfer at the upper plate while its effects on the rate of heat transfer at the lower plate are reversed. For high rotation, rotation accentuates the rate of heat transfer at the upper plate and inhibits heat transfer at the lower plate.

We now turn our attention to the response of dimensionless velocities (u_1, w_1) and induced magnetic field components (h_x, h_z) to different values of rotation parameter (K^2), Hall current parameter (m) and the Hartmann number (M^2) with pressure gradient prescribed as $R = 1$. The solutions are illustrated in Figs. 2 to 10 for the *velocity components* and Figs. 11 to 18 for the *induced magnetic field components*.

In Fig. 2, for small K^2 (weak rotational effects) the profiles indicate that the primary velocity component, u_1, *decreases* in the central regime of the channel with an increase in K^2 from 2 to 4, but then is increased with further increase in K^2 to 6, indicating that a particular channel rotation velocity (Ω) exists for which primary flow is minimized. Significant *flow reversal* is identified in the primary flow in the region near the lower plate. Clearly the channel centre primary velocity is minimized for $K^2 = 4$. It is also interesting to observe that a clear symmetry is sustained for $K^2 = 4$ and 6, but is absent for $K^2 = 2$. $K^2 = \Omega L^2/\nu$ defines the relative magnitude of the Coriolis and viscous hydrodynamic forces in the regime; increasing intensity of rotation therefore suppresses the primary flow in the channel central zone and serves to act as a regulatory mechanism in this vicinity. A more distributed flow profile is achieved with intermediate Coriolis forces which is of importance in practical operation of MHD rotating energy generator mechanisms. For $K^2 = 6$ a double peak arises in the primary profile with a trough at the channel centre, indicating an oscillatory nature to the flow i.e. unstable behaviour. The secondary velocity profiles are consistently symmetrical about the channel centerline ($\eta = 0$) for all $K^2 = 2, 4, 6$. Secondary velocity component, w_1, increases consistently in magnitude with increase in K^2 from 2 through 4 to 6; for $K^2 = 2, 4$, the profiles are parabolic; however for $K^2 = 6$ again a double-peak pattern is generated with a trough at the channel centre. Although for $K^2 = 2, 4$, the primary velocities exceed considerably the secondary component values, however this trend is reversed for $K^2 = 6$. In this latter case, w_1 magnitudes are noticeably in excess of the u_1 magnitudes across the channel. We note that Hall current is absent ($m = 0$) for all curves in Fig. 2 and that flow reversal i.e. backflow does not arise in the secondary flow. In Fig. 3, corresponding velocity profiles are illustrated, for large K^2, again *in the absence* of Hall current ($m = 0$). It is evident that velocity profiles are flattened having large values near the channel walls, which indicates the formation of boundary layers near the channel walls with reference to a rapidly rotating system. With an increases in K^2 from 50 through 75 to 81, the primary and secondary velocity profiles are progressively reduced i.e. both flows are decelerated. However for all values of K^2(strong rotation), the secondary flow (w_1) is an order of magnitude greater than the primary flow (u_1). Primary flow values are very small and follow a plateau distribution. However for all K^2 values the w_1 profiles exhibit a twin peak with a central plateau region; the peaks are amplified as K^2 ascends from 50 to 75 but then suppressed for $K^2 = 81$. As such the most evenly distributed secondary flow is achieved with very high rotational velocities of the system. Again it is apparent in consistency with other studies e.g. Mazumder [12], Prasad [13] and Bhat [14] that centrifugal inertial force (the Coriolis force) stabilizes both primary and secondary flow but markedly *accelerates* secondary momentum diffusion. In Fig. 4, velocity distributions are presented for weak rotation ($K^2 = 4$) for the effect of the Hall current parameter, m. Primary flow is initially increased as m rises from 0 (no Hall current) to 0.5; however with subsequent rise in m to 1.0 and 1.5, the values of u_1 principally in the zone near the channel centre are progressively reduced. While a

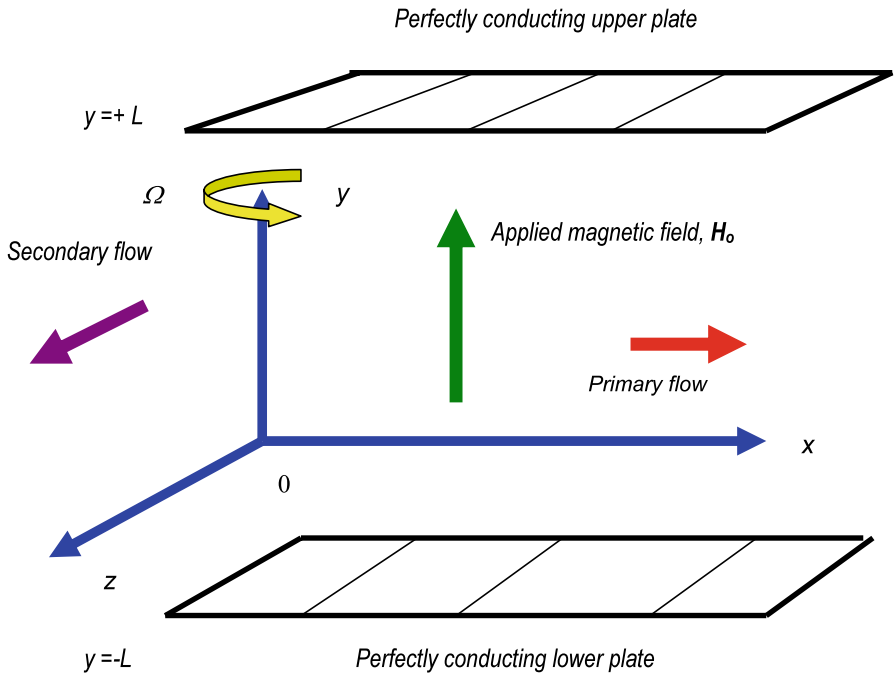

Fig. 1 Physical model and coordinate system

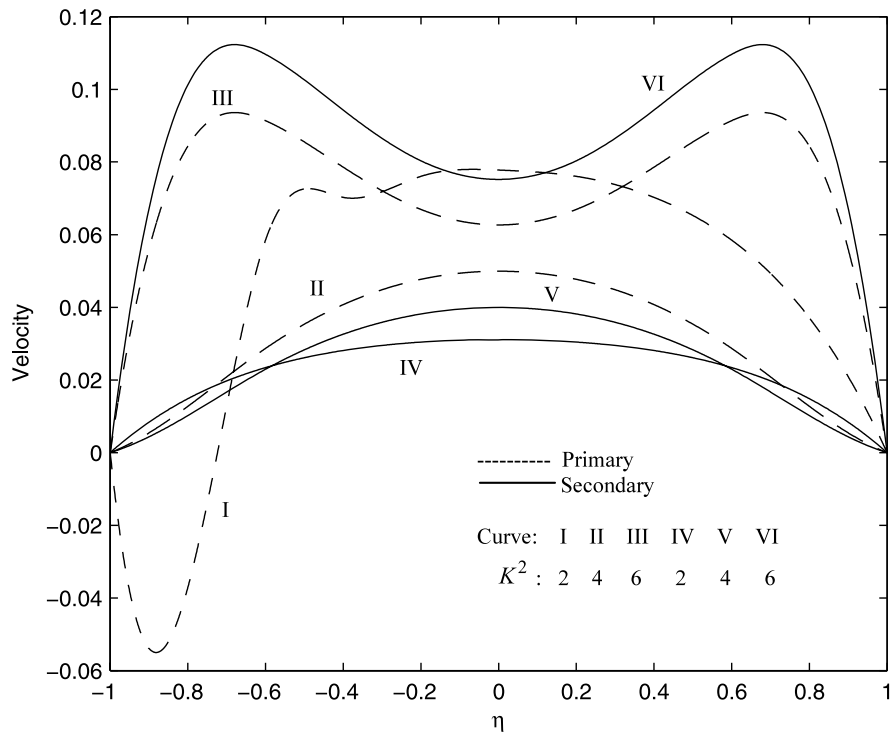

Fig. 2 Spatial velocity distribution for $M^2 = 10$, $m = 0$ (no Hall current)

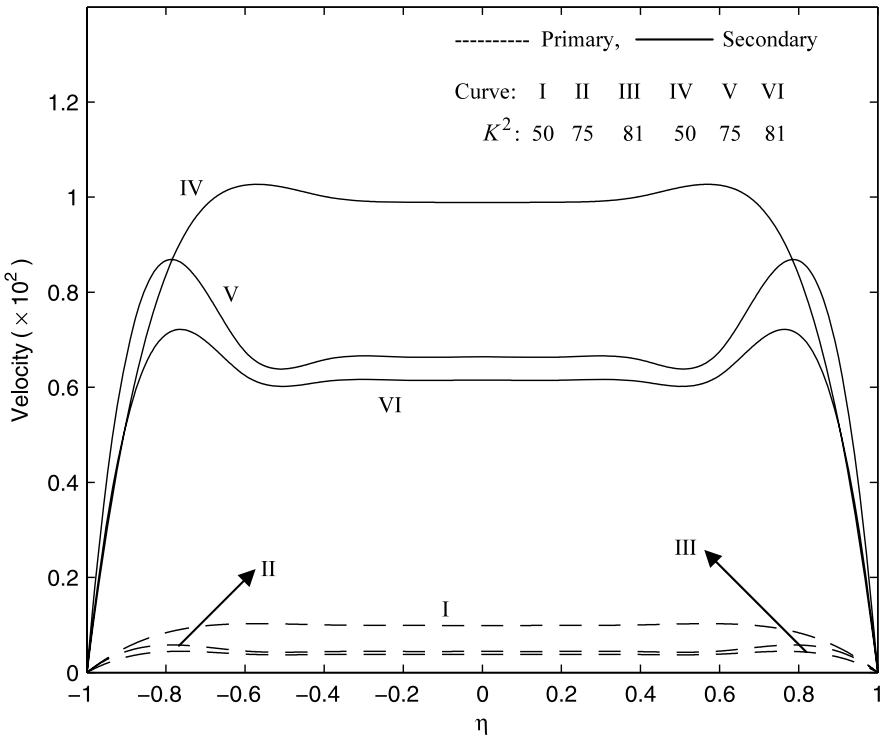

Fig. 3 Spatial velocity distribution for $M^2 = 10$, $m = 0$ (no Hall current)

smooth parabolic profile is witnessed for $m = 0.0$, for $m = 0.5$ (weak Hall current) the primary flow is disturbed across the channel width; for $m = 1.0$ and 1.5, the primary profiles are suppressed across the width of the channel. Strong Hall current therefore stifles the primary flow. Conversely there is a marked escalation in the secondary flow velocity, w_1 with increasing, m, since as pointed out in numerous MHD studies, the Hall current induces a *secondary* flow in the regime and as such the latter will respond more positively to increase in m values. Although individual peaks are maximum for $m = 1.0$, the secondary flow is consistently strongest across the channel span, for the maximum Hall current effect i.e. $m = 1.5$. An oblate parabolic profile is observed for $m = 1.5$ (curve VIII) demonstrating a strong boundary layer presence at the channel walls and a homogeneous distribution of secondary flow across the width of the channel. Figure 5 presents the velocity response for weak rotations ($K^2 = 4, 6$) but with $m = 0.5$. Comparing with the case without Hall current ($m = 0$) as shown in Fig. 2, we observe that primary flow for $K^2 = 4$ (curve I) is considerably perturbed when Hall current is present ($m = 0.5$); With $K^2 = 6$ however in Fig. 5 the flow is strongly stabilized across the channel span, whereas in the absence of Hall current (Fig. 2) it sustains an oscillatory profile across the channel. As such it can be deduced that better primary flow is obtained with *weak Hall current* present ($m = 0.5$) for intermediate values of the rotation parameter at the low end of the range. Conversely the secondary flow is generally increased substantially with Hall current present; values are elevated by an order of magnitude compared with Fig. 2. However for $K^2 = 4$ with $m = 0$, the w_1 profile is parabolic whereas for $m = 0.5$ it is oscillatory; similarly for $K^2 = 6$ and $m = 0$, the secondary profile is oscillatory whereas with $m = 0.5$, it is a flattened parabola. We can infer therefore that with Hall current present, secondary flow is stabilized with the maximum K^2 value.

Examining Fig. 6, we now consider the effect of *strong rotation* ($K^2 = 50, 75$ and 81, respectively) *with Hall current present* ($m = 0.5$), as this is of interest in high speed rotating MHD generator operations. We observe that primary flow (u_1) is decreased strongly with a rise in K^2 from 50 through 75 to 81; an enormous fall occurs in particular between $K^2 = 50$ and $K^2 = 75$. Similarly the secondary flow, with Hall

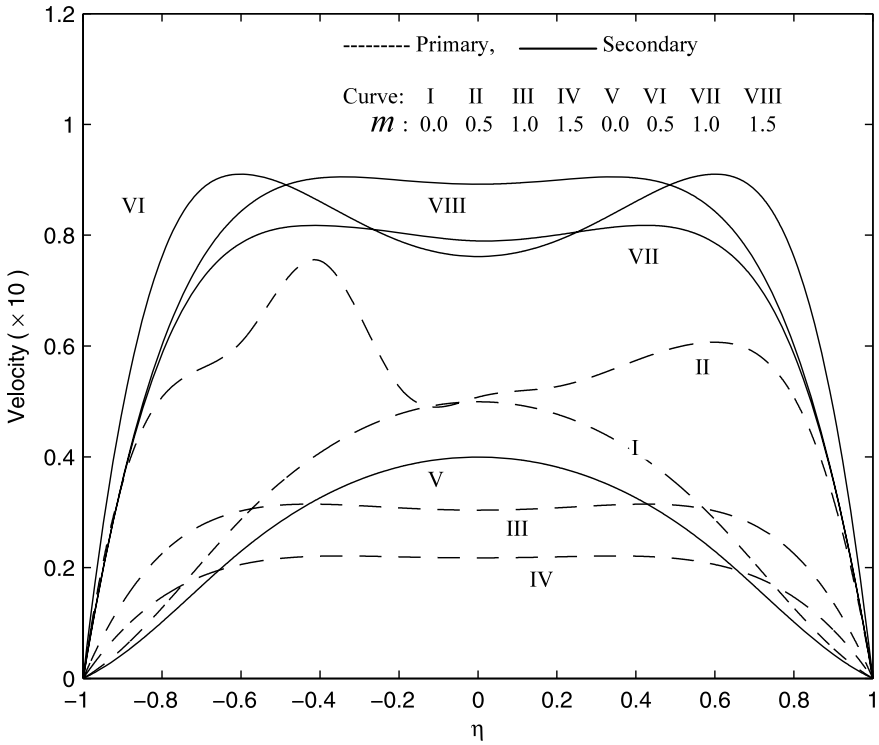

Fig. 4 Spatial velocity distribution for $M^2 = 10$, $K^2 = 4$ (weak rotation)

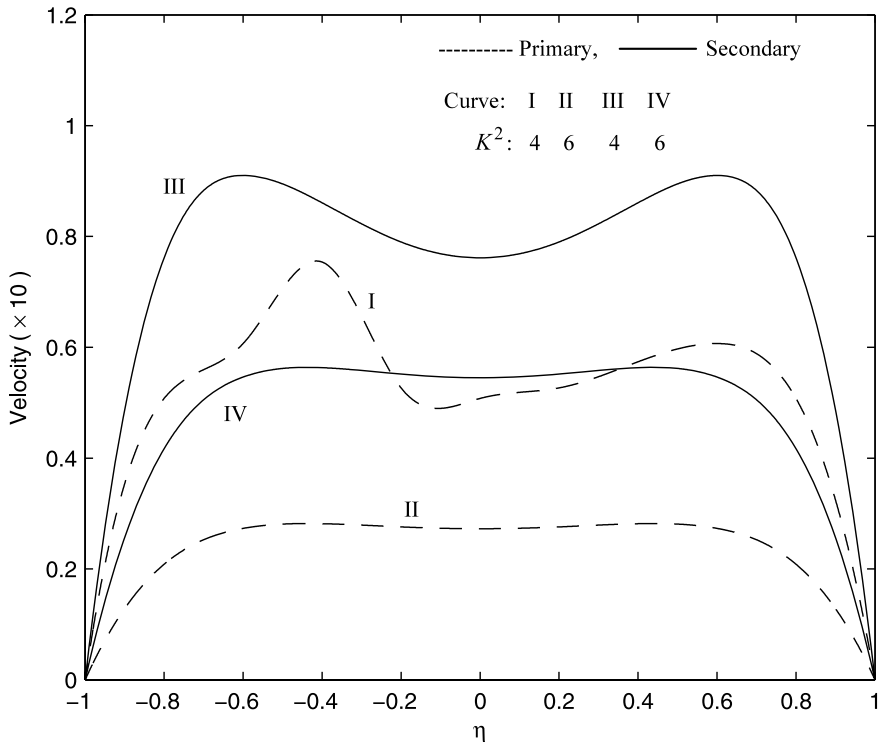

Fig. 5 Spatial velocity distribution for $M^2 = 10$, $m = 0.5$

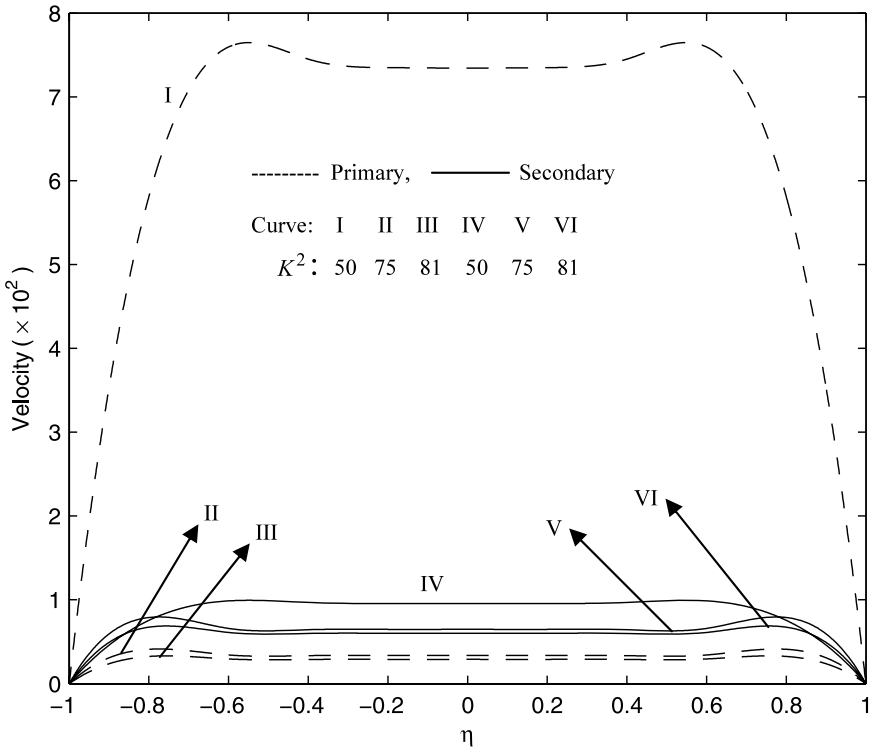

Fig. 6 Spatial velocity distribution for $M^2 = 10$, $m = 0.5$

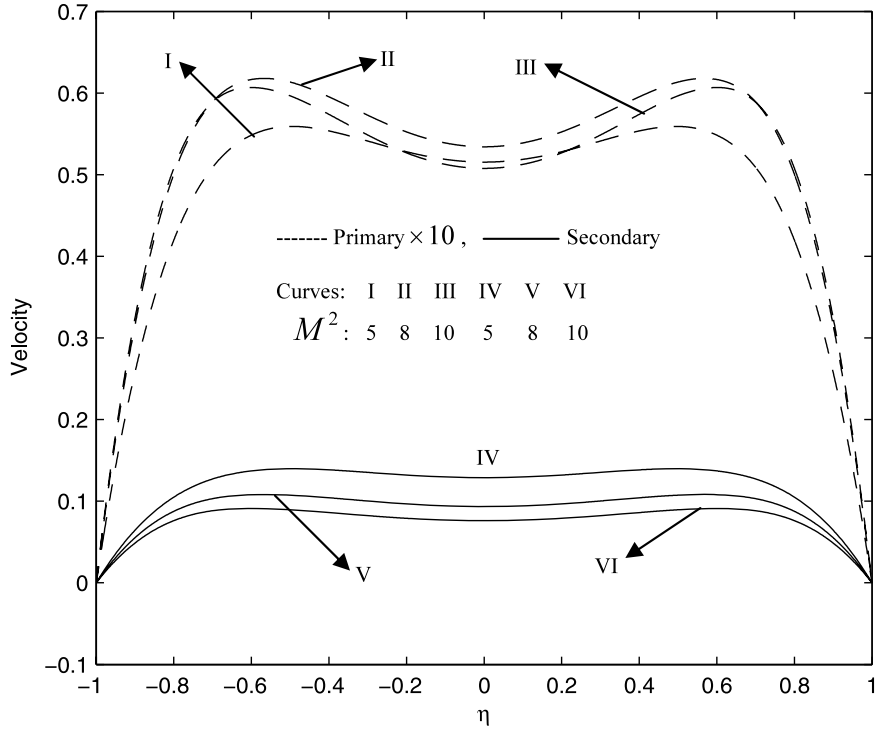

Fig. 7 Spatial velocity distribution for $K^2 = 4.0$, $m = 0.5$

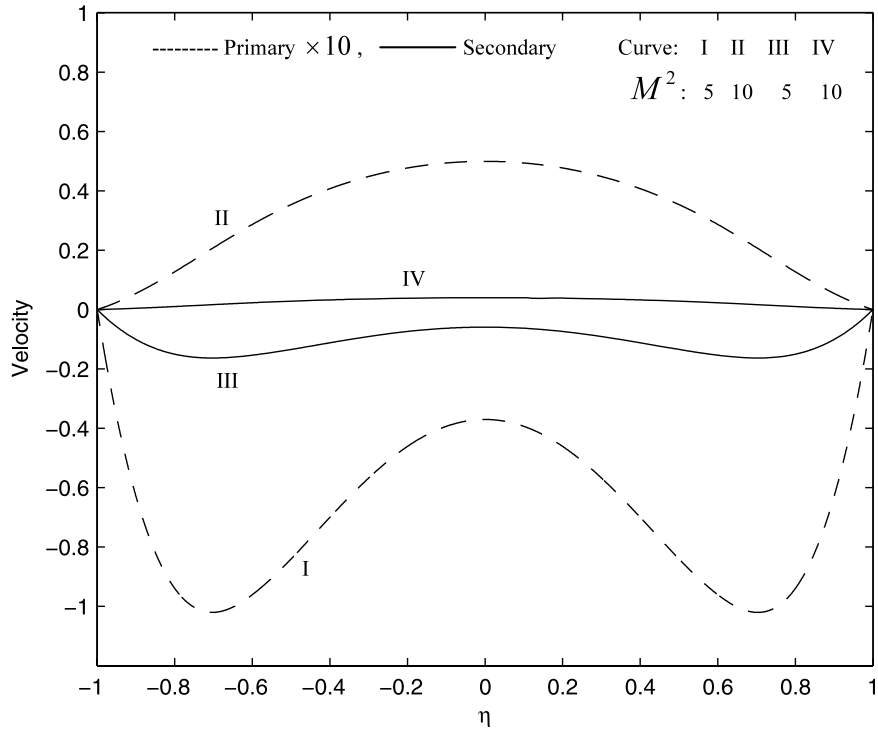

Fig. 8 Spatial velocity distribution for $K^2 = 4$, $m = 0$

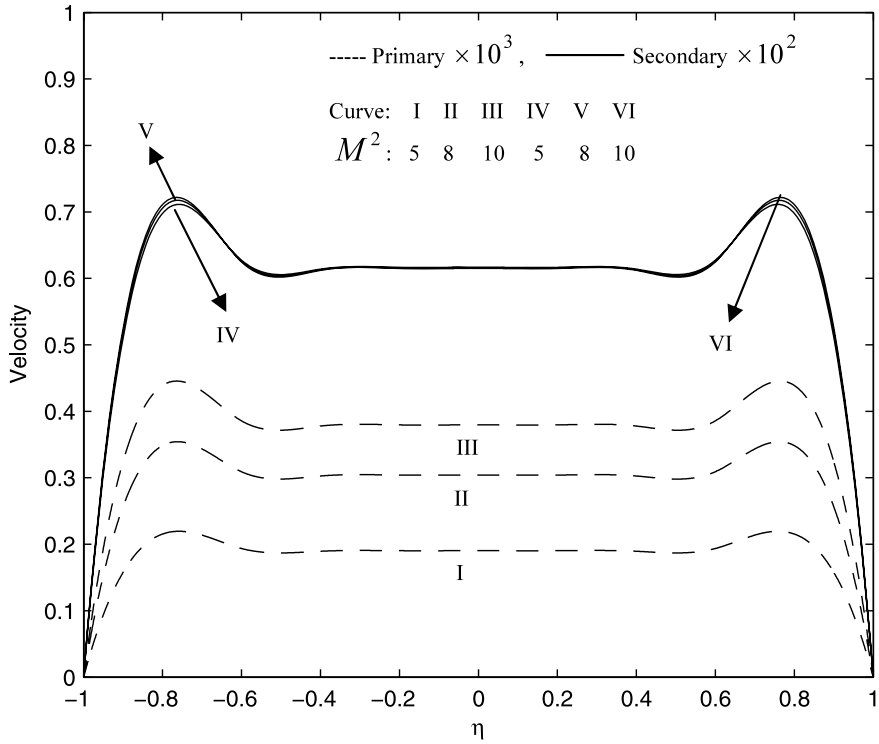

Fig. 9 Spatial velocity distribution for $K^2 = 81$, $m = 0$

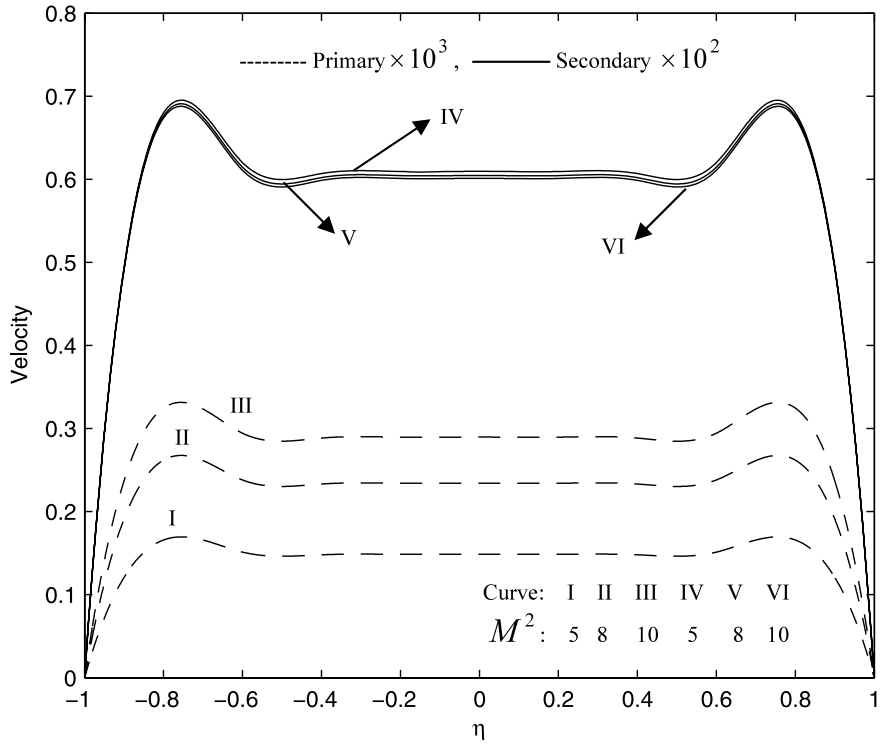

Fig. 10 Spatial velocity distribution for $K^2 = 81$, $m = 0.5$

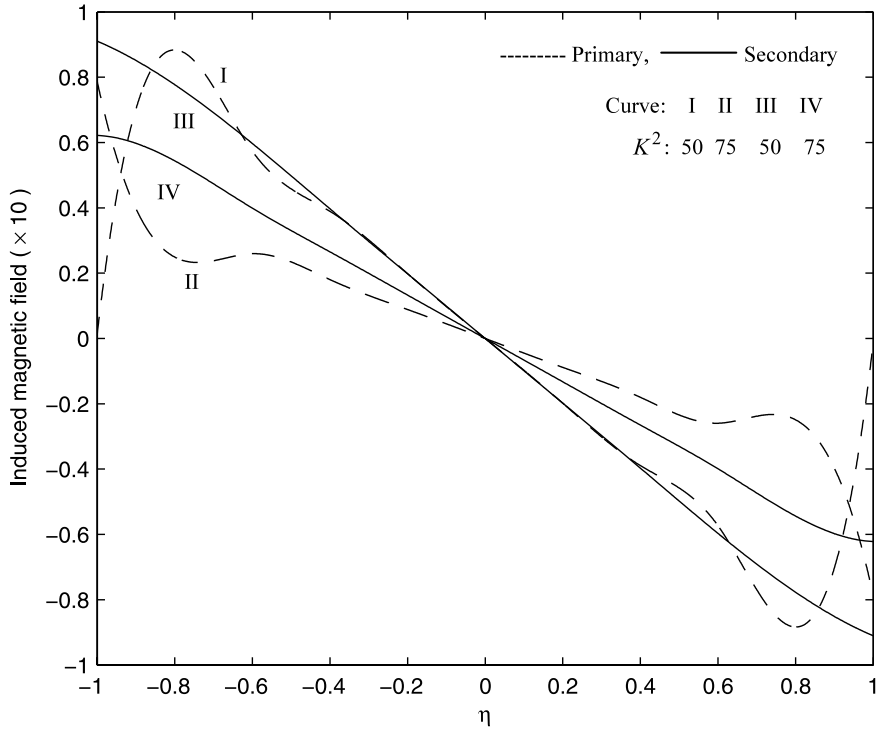

Fig. 11 Spatial induced magnetic field distribution; $M^2 = 10$, $m = 0.5$

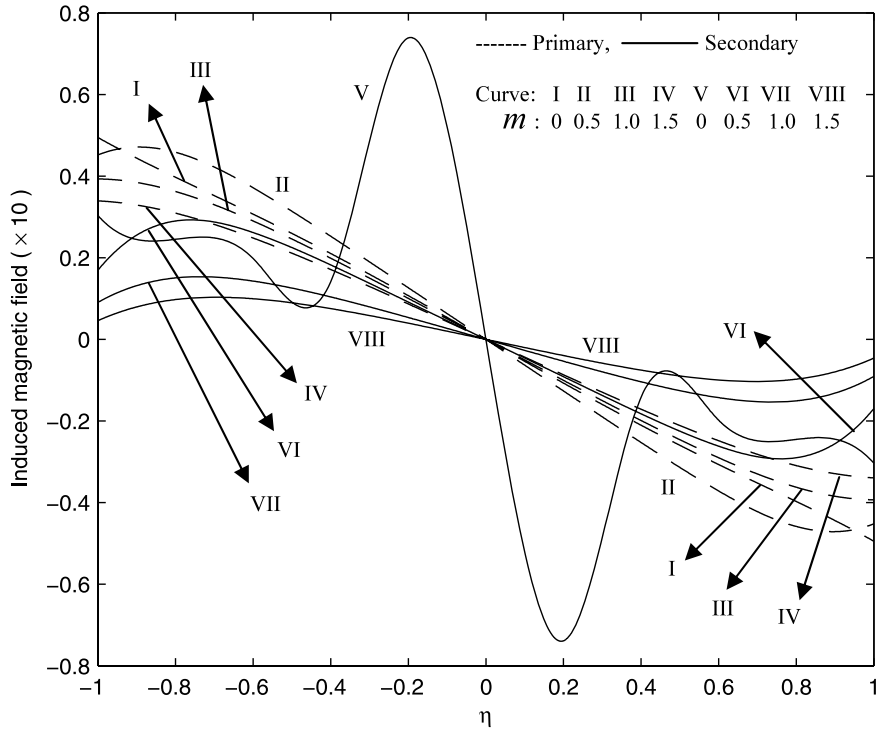

Fig. 12 Spatial induced magnetic field distribution; $M^2 = 10$, $K^2 = 4$

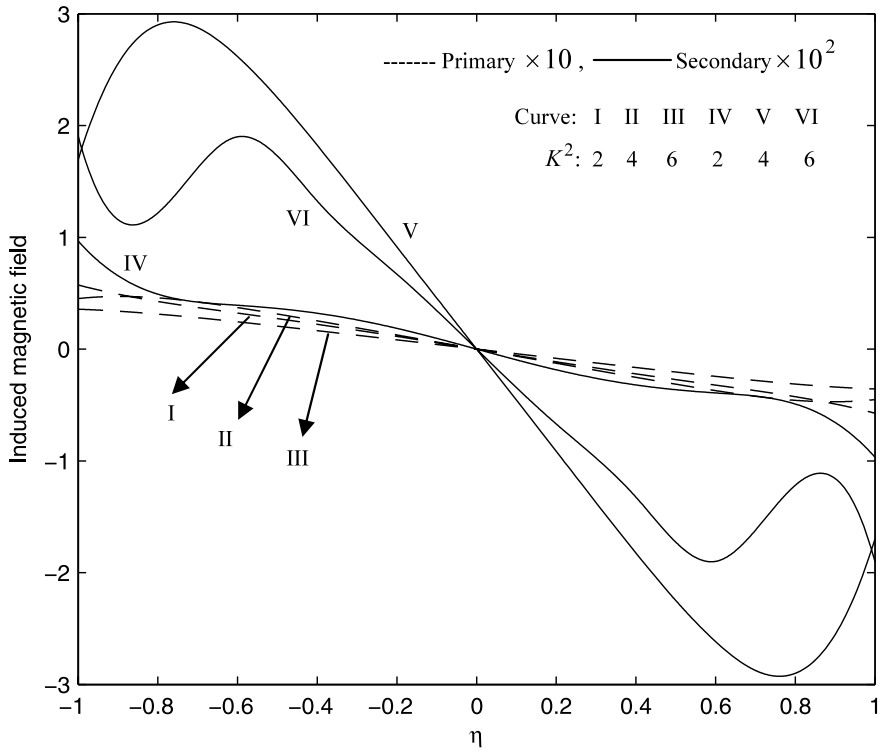

Fig. 13 Spatial induced magnetic field distribution; $M^2 = 10$, $m = 0$

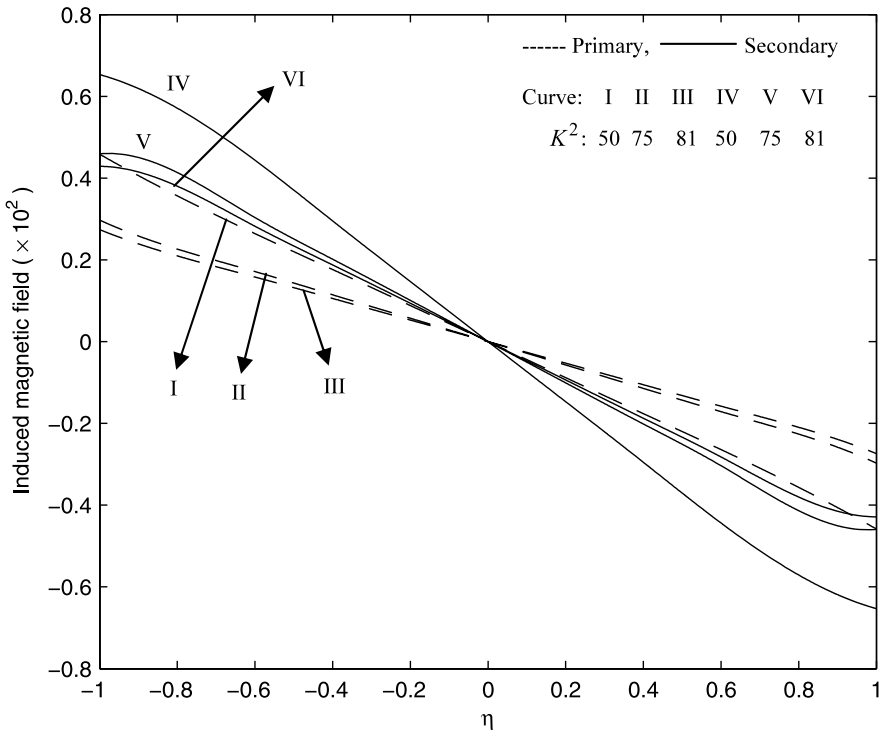

Fig. 14 Spatial induced magnetic field distribution; $M^2 = 10$, $m = 0$

current present, is also decreased with progressively greater values of K^2; but the effect is considerably less dramatic. Clearly high magnitude Coriolis forces therefore are counter-productive for both the primary and the secondary flow, even with Hall current present. Compared with the case for $m = 0$ (Fig. 3, curve I), we observe that for $K^2 = 50$, the primary flow is massively accelerated compared with the case when Hall current is present (curve I, Fig. 6). The maximum response corresponds to this case for Hall current being present. The secondary flow is only slightly retarded for all K^2 values as is the case when $m = 0$ (Fig. 3, curves IV, V, VI).

In Figs. 7 to 10, the effects of the square of the Hartmann number ($M^2 = 5, 8$ and 10, respectively) on the velocity evolution in the presence and absence of Hall current ($m = 0.5, 0$) for respectively weak rotation ($K^2 = 4$) and strong rotation ($K^2 = 81$) are shown. Figure 7 shows that primary flow velocity (u_1) is slightly accelerated with a rise in M^2 from 5 to 8 but thereafter reduced slightly e.g. at the channel centre u_1 values ascend from 0.051 to 0.053 but then fall to 0.0507. The secondary flow is consistently impeded with increasing M^2 i.e. the Lorentz body force serves to retard the secondary flow across the width of the channel. At the channel centre for example, w_1 values fall from 0.13 for $M^2 = 5$, to 0.09 for $M^2 = 8$ and to the minimum of 0.076 for $M^2 = 10$. Increasing transverse magnetic field therefore acts to decelerate secondary flow. We note however that the secondary flow, nevertheless, with Hall current present, despite the weak Coriolis forces ($K^2 = 4$) sustains values an order of magnitude in excess of the primary flow. The primary flow profiles are also weakly oscillatory in nature, whereas the secondary flow distribution is much more evenly distributed across the channel width. Figure 8 illustrates the velocity distributions again for weak rotation ($K^2 = 4$) for several M^2 values, but in the absence of Hall current ($m = 0$). In the absence of Hall current, for $M^2 = 5$ (curve I, Fig. 8) it is immediately apparent that a strong back flow arises in the primary flow across the channel width; a similar but weaker magnitude back flow is also present in the secondary flow for $M^2 = 5$ (curve III, Fig. 8). Both backflows are oscillatory in nature although the primary flow is evidently much more intense. No such back flow is computed in the presence of Hall current (curves I and IV, respectively, Fig. 7). With $M^2 = 10$

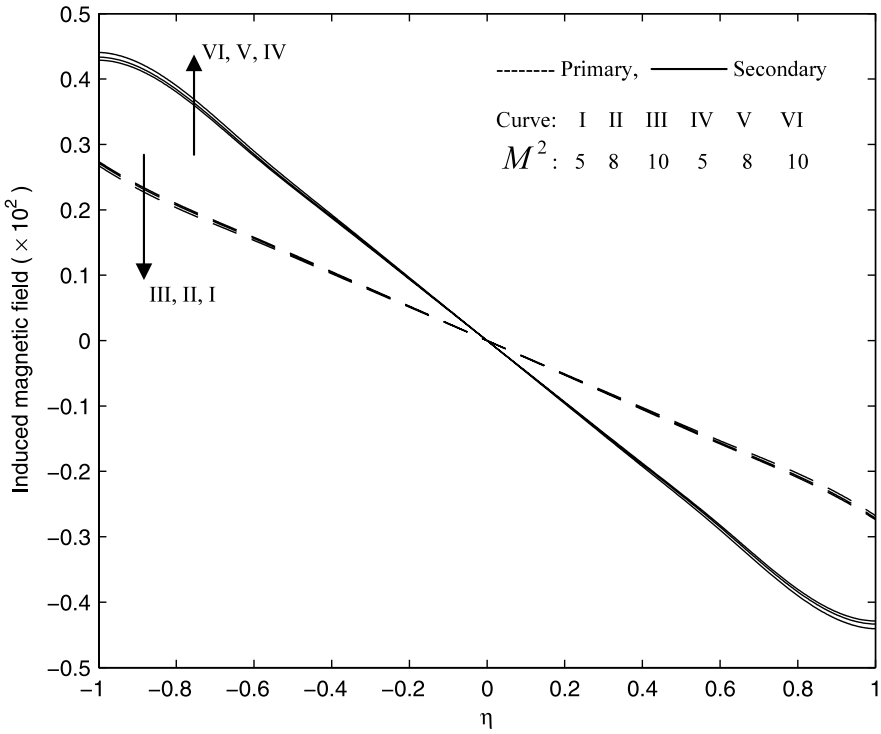

Fig. 15 Spatial induced magnetic field distribution; $K^2 = 81$, $m = 0$

(curve II, Fig. 8) this back flow is eliminated and the primary flow is actually accelerated, although compared with the $m = 0.5$ case (curve III, Fig. 7) it is effectively decelerated. However the secondary flow is decelerated to such an extent that it infact vanishes for $M^2 = 10$ (curve IV, Fig. 8), whereas clearly it is still present for $m = 0.5$ (curve VI, Fig. 7).

Figure 9 again illustrates the velocity distributions over the same increment of M^2 values, in the absence of Hall current ($m = 0$), but for *strong rotation* values ($K^2 = 81$). Compared with the case for weak rotation (Fig. 8) both the primary and secondary velocities are several orders of magnitude lower for strong rotation. *Back flow* however *does not* arise for *any* value of the square of the Hartmann number. Although the secondary flow velocity (w_1) values are low they are considerably higher than the primary flow velocity values across the channel. Increasing M^2 values consistently boost the primary flow throughout the channel; however the secondary flow is very weakly affected with an increase in M^2 from 5 through 8 to 10. In all cases a double peak profile, with peaks near the channel walls and a plateau distribution across the central section of the channel, is observed, indicating that very strong rotation actually regulates both the primary and secondary flow, producing a more even distribution.

In Fig. 10, the velocity distributions over the same change in M^2 values, but with weak Hall current acting ($m = 0.5$), and also strong rotation values ($K^2 = 81$), are illustrated. A similar trend is observed for the primary velocity, u_1, which continuously is elevated with increasing M^2 values; secondary velocity is however consistently diminished since the magnetic field creates a transverse retarding body force (Lorentz drag) opposite to the secondary flow direction in the channel. High Coriolis forces ($K^2 = \Omega L^2/\nu$) also tend to oppose the secondary flow inhibiting its development. The fact that the two sets of curves in Figs. 9 and 10, have similar magnitudes also indicates that strong rotation dominates over the effect of Hall current which exerts an almost negligible effect. Similar deductions were arrived at by Seth and Ghosh [31], Linga Raju and Ramana Rao [32] and also Ram et al. [33].

We shall now consider the effects of K^2, m and M^2 on the *primary and secondary induced magnetic field*

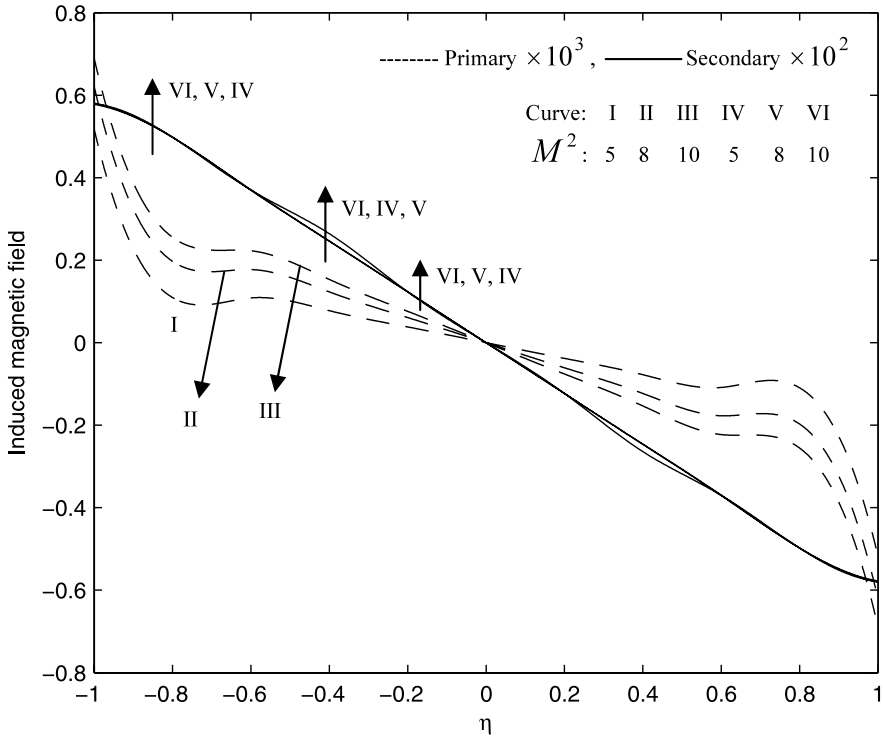

Fig. 16 Spatial induced magnetic field distribution; $K^2 = 81$, $m = 0.5$

components in the channel, all of which are presented in Figs. 11 to 18.

Figure 11 shows the evolution of the components of the induced magnetic field, h_x, h_z across the channel, for weak Hall current ($m = 0.5$), strong magnetic field ($M^2 = 10$) and various strong rotation values (equivalent to weak Ekman numbers) i.e. $K^2 = 50, 75$ respectively. For both primary and secondary magnetic field distributions, there is a strong magnetic flux reversal (*magnetic back flow*) in the upper channel half space ($0 < \eta < 1$) which is totally absent in the lower channel half space ($-1 < \eta < 0$). Magnitudes of the primary magnetic field component (h_x) for $K^2 = 75$, are also somewhat greater than the secondary component (h_z) in the upper channel half-space; the reverse trend is apparent in the lower channel half-space. An increase in K^2 from 50 to 75 markedly reduces the primary induced field in the lower channel half space but increases it in the upper channel half space. A similar pattern is computed for the secondary induced field. There is also a reflective symmetry apparent for the profiles about the channel centre line.

The effects of Hall current parameter (m) on h_x and h_z are shown for weak rotation ($K^2 = 4$) and strong magnetic field ($M^2 = 10$) in Fig. 12. The reflective symmetry about the channel centre line is again apparent in consistency with conservation of magnetic induction. Increasing Hall current initially enhances primary induced magnetic field component value in the lower channel half space as m increases from 0 to 0.5 (curves I and II respectively); however with a subsequent increase in m to 1.0 and finally 1.5, the h_x values are clearly lowered in the region $-1 < \eta < 0$. The exact opposite response is witnessed in the upper channel half space $0 < \eta < 1$. *In all cases the profiles descend smoothly from the lower plate to the upper plate*. Magnetic back flow occurs in the upper channel half space for all values of m, although it is progressively stifled with increasing m. Secondary magnetic induction, h_z, is decreased in the lower channel half space as m rises from 0.5 through 1.0 to 1.5 (curves VI, VII, VIII); however for $m = 0$ a higher h_z arises at the lower plate and a much higher peak is observed near the channel centerline—the response is infact oscillatory owing to the stabilizing influence of Hall cur-

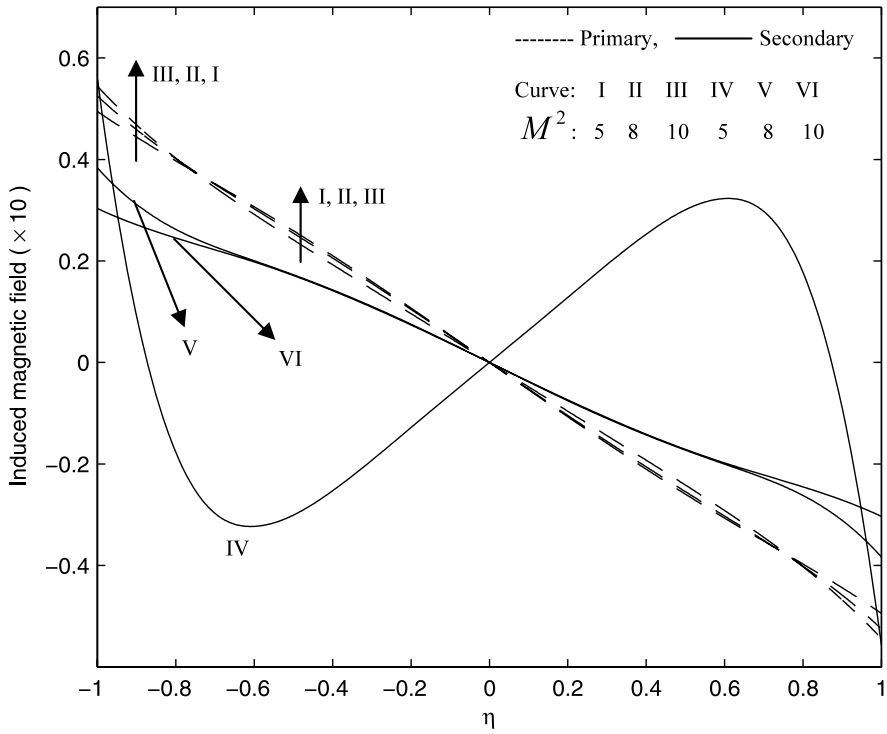

Fig. 17 Spatial induced magnetic field distribution; $K^2 = 4$, $m = 0$

rent being absent in *curve V*. In the upper channel half space significant magnetic back flow i.e. flux reversal is apparent but again this is inhibited considerably with an increase in Hall current parameter. The weakest reversal in secondary field therefore corresponds as expected to the strongest Hall current ($m = 1.5$, curve VIII).

Figure 13 shows the change in h_x, h_z, with weak rotation values, for no Hall current and strong magnetic field ($M^2 = 10$). An increase in K^2 from 2 through 4, to 6, progressively inhibits the primary induced magnetic field (h_x) in the lower channel half space; secondary induced magnetic field component (h_z) is initially increased strongly as K^2 rises from 2 to 4, but then decreased considerably. An oscillatory response is also observed for $K^2 = 6$ (curve VI) again indicating that greater rotation destabilizes the secondary magnetic induction field. Magnitudes of primary induction are very low across the channel; secondary induction values are much higher. Magnetic flux reversal again arises in the upper channel half space, but not in the lower channel half space and is particularly prominent for the secondary induction (h_z).

Figure 14 depicts the change in h_x, h_z, with strong rotation values ($K^2 = 50, 75, 81$), again for no Hall current and strong magnetic field ($M^2 = 10$); in this case they are directly comparable therefore to Fig. 13. A substantial decrease in both primary and secondary magnetic induction values is observed at higher rotational parameter values. The trends of the profiles are similar to the weak rotation case in that magnetic flux reversal is confined to the upper channel half space only. However no periodic behaviour arises in the secondary flow at higher rotation parameter (lower Ekman number) values indicating that the magnetic induction is more evenly distributed at higher rotational velocities of the system. As such very strong rotational body forces are more effective in impeding the development of the magnetic induction in the regime compared with weaker rotational body forces (Coriolis forces).

Finally in Figs. 15 to 18, the effect of the applied magnetic field strength, embodied in the Hartmann number squared, M^2, on h_x and h_z profiles, are shown, for strong rotation ($K^2 = 81$) without Hall current ($m = 0$, Fig. 15) and with Hall current ($m = 0.5$,

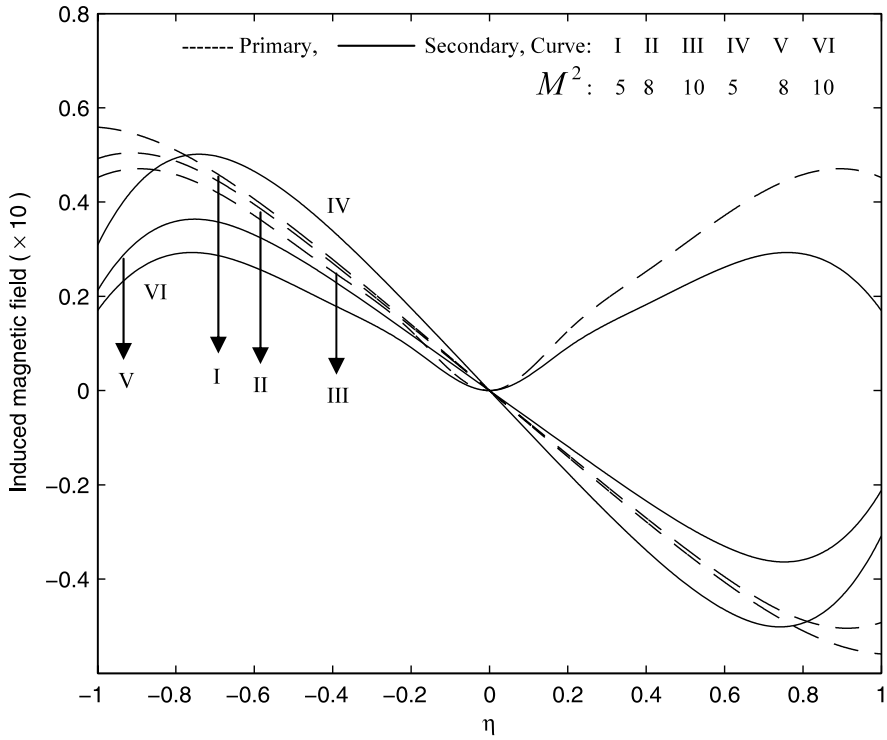

Fig. 18 Spatial induced magnetic field distribution; $K^2 = 4$, $m = 0.5$

Fig. 16) and for weak rotation ($K^2 = 4$) again without Hall current ($m = 0$, Fig. 17) and with Hall current ($m = 0.5$, Fig. 18).

Figure 15 indicates that increasing M^2 values slightly enhance the primary component (h_x) in the lower channel half space but suppresses the secondary component (h_z), with the reverse observed in the upper channel half space. Hence again significant magnetic flux reversal arises only in the upper channel half space, but this is reduced fractionally for the secondary magnetic induction and increased in the primary magnetic induction with a rise in M^2. With Hall current present ($m = 0.5$) the primary magnetic induction is oscillatory in nature for $K^2 = 81$, and strongly affected with a rise in M^2, as shown in Fig. 16, whereas the secondary induction is not significantly affected. Magnetic flux reversal however again is restricted purely to the upper channel half space even with Hall current present.

In Fig. 17 we observe that at weaker rotation, $K^2 = 4$, without Hall current, the primary magnetic induction is reduced with increasing M^2 very close to the lower plate, a trend which is reversed further from the lower plate; in the upper channel half space the exact opposite is observed. Primary magnetic flux reversal is solely confined to the upper channel half space. Conversely in the secondary magnetic induction field, significant magnetic flux reversal arises in the lower channel half space for $M^2 = 5$ (curve IV), but this effect is eliminated for $M^2 = 8$ and 10 (curves V and VI). With Hall current present, Fig. 18 shows that irrespective of M^2 value, magnetic flux reversal is isolated to the upper channel halfspace. It is also interesting to note that while reflective symmetrical profiles exist for $M^2 = 5, 8$ for both the primary and secondary magnetic induction so that positive h_x and h_z arise in the lower channel half space and negative values in the upper channel half space, for the single case of a maximum applied magnetic field strength, $M^2 = 10$, no magnetic reversal occurs anywhere across the channel for either the primary or secondary fields. A strong magnetic field, with Hall current present at low rotational intensity ($K^2 = 4$) would therefore appear to damp the magnetic induction negating magnetic flow reversal.

7 Conclusions

A theoretical study has been conducted of the steady, hydromagnetic, viscous, Newtonian flow in a rotating channel under a transverse magnetic field, with heat transfer and Hall currents, present. Both viscous and Joule dissipation effects have been incorporated in the heat balance equation. Non-dimensional closed-form solutions have been derived for the primary and secondary velocity distribution and induced magnetic field component distribution across the channel width. Asymptotic behavior of the solution for velocity has also been addressed in order to elucidate the boundary layer-type flow for large values of the Hartmann hydromagnetic parameter, M^2 and the inverse Ekman number, K^2. The effects of Hall current have been shown to exert a key role on the flow dynamics and evolution of magnetic induction fields. The rate of heat transfer has been analyzed for both weak and strong rotation scenarios and some interesting features of the flow identified. Magnetic flux reversal has been shown to arise for particular combinations of M^2, K^2 and m and to be eliminated only for $K^2 = 4$, $M^2 = 10$ and $m = 0.5$. In the current study which has applications in MHD energy generator systems, for example, a single-phase Newtonian model has been employed. Future studies will consider non-Newtonian aspects and also two-phase (fluid–particle suspension) hydromagnetics. Also numerical simulations will be performed and communicated imminently.

Appendix

$$a_1 = \cosh\alpha\cos\beta, \qquad b_1 = \sinh\alpha\sin\beta$$
$$a_2 = a_1/\left(a_1^2 + b_1^2\right), \qquad b_2 = b_1/\left(a_1^2 + b_1^2\right),$$
$$a_3 = \alpha/\left(\alpha^2 + \beta^2\right), \qquad b_3 = \beta/\left(\alpha^2 + \beta^2\right),$$

$$a_4 = 4\alpha\beta K^2/\left(\alpha^2 + \beta^2\right)^2,$$
$$b_4 = 2K^2\left(\alpha^2 - \beta^2\right)/\left(\alpha^2 + \beta^2\right)^2,$$
$$c_1 = \frac{1}{2}\left(a_3^2 + b_3^2\right)\left(a_2^2 + b_2^2\right),$$
$$c_2 = \frac{1}{2}\left(a_2^2 + b_2^2\right)\left(1 + 2a_4 + a_4^2 + b_4^2\right),$$

$$c_3 = 2a_2\left\{(1 + 2a_4) + \left(a_4^2 + b_4^2\right)\right\},$$
$$c_4 = 2b_2\left\{(1 + 2a_4) + \left(a_4^2 + b_4^2\right)\right\},$$
$$c_5 = \left\{(1 + 2a_4) + \left(a_4^2 + b_4^2\right)\right\},$$
$$c_6 = c_1/4\alpha^2, \qquad c_7 = c_1/4\beta^2,$$
$$c_8 = c_2/4M^2\alpha^2, \qquad c_9 = c_2/4M^2\beta^2,$$
$$c_{10} = c_3\alpha/M^2\left(\alpha^2 + \beta^2\right)^2,$$

$$c_{11} = c_3\beta/M^2\left(\alpha^2 + \beta^2\right)^2,$$
$$c_{12} = c_4\alpha/M^2\left(\alpha^2 + \beta^2\right)^2,$$
$$c_{13} = c_4\beta/M^2\left(\alpha^2 + \beta^2\right)^2,$$
$$c_{14} = c_{13} - c_{10}, \qquad c_{15} = c_{11} + c_{12},$$
$$c_{16} = c_6 + c_8, \qquad c_{17} = c_7 - c_9.$$

References

1. Vogin C, Alemany A (2007) Analysis of the flow in a thermo-acoustic MHD generator with conducting walls. Eur J Mech B 26(4):479–493
2. Thakur C, Mishra RB (1988) On steady plane rotating hydromagnetic flows. Astrophys Space Sci 146(1):89–97
3. Friedrich J, Kupfer C, Fischer B, Muller G (1997) Influence of rotating magnetic fields on heat and species transport in crystal growth by the vertical gradient freeze method. In: 3rd Int. Conf. Transport Phenomena in Magnetohydrodynamic and Electroconducting Flows, Aussios, France, 22–26 September, pp 439–444
4. Yasuda H (2007) Applications of high magnetic fields in materials processing. In: Molokov, S., Moreau, R., Moffatt, K. (eds), Magnetohydrodynamics: historical evolution and trends, Fluid mechanics and its applications, vol 80, Part IV, pp 329–344
5. Zueco J, Anwar Bég O (2009, submitted) Network numerical simulation of hydromagnetic squeeze film flow between rotating disks with magnetic Reynolds number effects. Eur J Mech B
6. Han SM, Wu ST, Dryer M (1988) A three-dimensional, time-dependent numerical modeling of super-sonic, super-alfvénic MHD flow. Comput Fluids 16(1):81–103
7. Alfven H (1953) Cosmical electrodynamics. Oxford University Press, Reprint
8. Todd L (1967) Hartmann flow in an annular channel. J Fluid Mech 28:371–384
9. Vidyanidhi V, Ramana Rao VV (1968) Hydromagnetic flow in a rotating straight pipe. J Phys Soc Jpn 25(6):1694–1700
10. Nanda RS, Mohanty HK (1971) Hydromagnetic flow in a rotating channel. Appl Sci Res 24:65–78
11. Acheson DJ, Hide R (1973) Hydromagnetics of rotating fluids. Rep Prog Phys 36:159–221
12. Mazumder BS (1977) Effect of wall conductances on hydromagnetic flow and heat transfer in a rotating channel. Acta Mech 28:85–99

13. Prasad VB, Rao VVR (1978) Hydromagnetic flow between two parallel porous walls in a rotating system. Def Sci J 28:51–58
14. Bhat JP (1982) Heat transfer in MHD flow in a rotating channel. Czech J Phys 32(9):1050–1055
15. Singh SN, Tripathi DD (1987) Hodograph transformation in steady plane rotating MHD flows. Appl Sci Res 43(4):347–353
16. Kishore Kumar S, Thacker WI, Watson LT (1988) Magnetohydrodynamic flow and heat transfer about a rotating disk with suction and injection at the disk surface. Comput Fluids 16(2):183–193
17. Nagy T, Demendy Z (1993) Influence of wall properties on Hartmann flow and heat transfer in a rotating system. Acta Phys Hung 7(2–4):291–310
18. Ghosh SK (1993) Unsteady hydromagnetic flow in a rotating channel with oscillating pressure gradient. J Phys Soc Jpn 62(11):3893–3903
19. Ghosh SK, Pop I (2002) A note on a hydromagnetic flow in a slowly rotating system in the presence of an inclined magnetic field. Magnetohydrodynamics 38(4):377–384
20. Asghar SKH, Nadeem S, Hayat T (2004) Magnetohydrodynamic rotating flow of a second grade fluid with a given volume flow rate variation. Meccanica 39:483–488
21. Roy S, Takhar HS, Nath G (2004) Unsteady MHD flow on a rotating cone in a rotating fluid. Meccanica 39:271–283
22. Hayat T, Hameed MI, Asghar S, Siddiqui AM (2004) Some steady MHD flows of the second order fluid. Meccanica 39(4):345–355
23. Xu H, Liao S-H (2006) Series solutions of unsteady MHD flows above a rotating disk. Meccanica 41:599–609
24. Asghar SKH, Hayat T (2007) The effect of the slip condition on unsteady flow due to non-coaxial rotations of disk and a fluid at infinity. Meccanica 42:141–148
25. Lighthill Sir MJ (1960) Studies on MHD waves and other anisotropic wave motion. Phil Trans R Soc, Lond 252A:397–430
26. Sato H (1961) The Hall effect in the viscous flow of ionized gas between parallel plates under transverse magnetic field. J Phys Soc Jpn 16(7):1427–1435
27. Shang JS, Surzhikov ST, Kimmel R, Gaitonde D, Menart J, Hayes J (2005) Mechanisms of plasma actuators for hypersonic flow control. Prog Aerosp Sci 41(8):642–668
28. Fife J (1998) Hybrid-PIC Modeling and electrostatic probe survey of Hall thrusters. PhD Thesis, Department of Aeronautics and Astronautics, Massachusetts Institute of Technology (MIT), USA
29. Ishikwa M, Yuhara M, Fujino T (2007) Three-dimensional computation of magnetohydrodynamics in a weakly ionized plasma with strong MHD interaction. J Mater Process Technol 181(1–3):254–259
30. Nishihara M, Jiang N, Rich JW, Lempert WR, Adamovich IV, Gogineni S (2005) Low-temperature supersonic boundary layer control using repetitively pulsed magnetohydrodynamic forcing. Phys Fluids 17:106102–106112
31. Seth GS, Ghosh SK (1986) Effect of Hall currents on unsteady hydromagnetic flow in a rotating channel with oscillating pressure gradient. Indian J Pure Appl Math 17(6):819–826
32. Linga Raju T, Ramana Rao VV (1993) Hall effects on temperature distribution in a rotating ionized hydromagnetic flow between parallel wall. Int J Eng Sci 31(7):1073–1091
33. Ram PC, Singh A, Takhar HS (1995) Effects of Hall and ionslip currents on convective flow in a rotating fluid with wall temperature oscillation. Magnetohydrodyn Plasma Res J 5:1–16
34. Takhar HS, Jha BK (1998) Effects of Hall and ionslip currents on MHD flow past an impulsively started plate in a rotating system. Magnetohydrodyn Plasma Res J 8:61–72
35. Takhar HS, Chamkha AJ, Nath G (2002) MHD flow over a moving plate in a rotating fluid with magnetic field, Hall currents and free stream velocity. Int J Eng Sci 40:1511–1527
36. Ghosh SK (2002) Effects of Hall current on MHD Couette flow in a rotating system with arbitrary magnetic field. Czech J Phys 52(1):51–63
37. Ghosh SK, Pop I (2003) Hall effects on unsteady hydromagnetic flow in a rotating system with oscillating pressure gradient. Int J Appl Mechan Eng 8(1):43–56
38. Ghosh SK, Pop I (2004) Hall effects on MHD plasma Couette flow in a rotating environment. Int J Appl Mech Eng 9(2):293–305
39. Hayat T, Wang Y, Hutter K (2004) Hall effects on the unsteady hydromagnetic oscillatory flow of a second grade fluid. Int J Non-Linear Mech 39(6):1027–1037
40. Naroua H (2007) A computational solution of hydromagnetic-free convective flow past a vertical plate in a rotating heat-generating fluid with Hall and ion-slip currents. Int J Numer Methods Fluids 53(10):1647–1658
41. Naroua H, Takhar HS, Ram PC, Beg TA, Anwar Beg O, Bhargava R (2007) Transient rotating hydromagnetic partially-ionized heat-generating gas dynamic flow with Hall/Ion-slip current effects: finite element analysis. Int J Fluid Mech Res 34(6):493–505
42. Bég OA, Zueco J, Takhar HS (2009) Unsteady magnetohydrodynamic Hartmann–Couette flow and heat transfer in a Darcian channel with Hall current, ionslip, viscous and Joule heating effects: Network numerical solutions. Commun Nonlinear Sci Numer Simul 14:1082–1097
43. Sutton GW, Sherman A (1965) Engineering magnetohydrodynamics. MacGraw-Hill, New York